Recent Advances in Electrochromic Smart Fenestration

Cai, Guofa; Eh, Alice Lee‐Sie; Ji, Lin; Lee, Pooi See

2017

Cai, G., Eh, A. L.-S., Ji, L., & Lee, P. S. (2017). Recent Advances in Electrochromic Smart Fenestration. Advanced Sustainable Systems, 1(12), 1700074-.

https://hdl.handle.net/10356/88794

https://doi.org/10.1002/adsu.201700074

WILEY-VCH

DOI: 10.1002/ ((please add manuscript number))
Article type: ((**Review**))

Recent advances in electrochromic smart fenestration

*Guofa Cai, Alice Lee-Sie Eh, Lin Ji, and Pooi See Lee**

Dr. G. F. Cai, A. L-S. Eh, L. Ji, Prof. P. S. Lee

School of Materials Science and Engineering

Nanyang Technological University

50 Nanyang Avenue, Singapore 639798, Singapore

E-mail: pslee@ntu.edu.sg

Keywords: smart window, electrochromism, multifunctional device, energy storage, sustainable energy

Fenestration such as window plays a key role in modern architecture as it has enormous impact on the energy efficiency and comfort to its occupants in the building. Herein, current state-of-art strategies of nanostructured electrochromic materials, the fabrication of large scale smart windows, rational design of multifunctional smart chromogenic devices and their performances are highlighted. Moreover, the challenges from materials selection to smart windows performances are discussed and feasible solutions are provided. Development of a novel, simple and economical synthesis of electrochromic materials is the first step in realizing high-performance smart window. In addition, electrolyte, packaging materials and judicious design of the fabrication process also play critical roles in the development of multifunctional and energy-efficient smart windows. Finally, the concept of energy-efficient multifunctional smart windows is addressed in which the smart windows are powered by sustainable energy in daytime, while the windows dynamically control the solar radiation into the building through transmittance modulation, enabling adjustable occupant's privacy. Sustainable energy can be stored in the smart windows during daytime and can be discharged to power other electronic devices at night.

We envision that this review shall promote a rapid development on electrochromic materials and novel multifunctional smart windows.

1. Introduction

Sustainable energy production, storage, conservation, and management are garnering increasing concerns due to the depletion of fossil fuels reserves.[1-3] Energy conservation and energy efficiency management in buildings are very important because more than 40% of the total primary energy are used for cooling, heating, ventilation and other electrical appliances in developed countries.[4, 5] Window plays an important role in the energy efficiency of buildings, besides providing visual comfort.[6, 7] Compared with ordinary static windows, smart windows could significantly improve the energy efficiency of buildings as well as provide a comfortable environment by dynamically modulating solar irradiation and solar heating flux into buildings by reversibly switching their optical properties between transparent state and blocking state. Energy Efficiency Index (EEI) is an important performance parameter to compare and track the energy consumption in buildings. EEI can be expressed as the ratio of the energy input to the factor related to the energy expenditure of component.[8] González *et al.* defined EEI as the ratio between the performance (in terms of energy consumption or carbon dioxide emissions) of an actual building to that of a reference building.[9] Typically, EEI is often cited in kWh/m^2/year which characterized the total energy consumption used in a building per unit floor area per year. The energy saving targets are always based on the lowest EEI for the building. According to the research involving 73 case studies from 13 countries of Ramesh *et al.*,[10] the range of EEI were between 150 and 400 kWh/m^2/year and between 250 and 550 kWh/m^2/year (primary) for residential and office buildings, respectively. Meanwhile, the smart fenestration concepts have been adopted in transportation industry such as automobiles and aircrafts, with the goals of

tuning visible transmittance autonomously and versatile heat management. The chromogenic applications have also been extended to the preservation efforts in art and history artefacts exhibitions or museums to adjust the light transmittance in protection of the exhibits.

Typically, three different technologies with distinctive external stimuli are known for smart windows and have been made available on the commercial market: chromic materials, liquid crystals (LC) and electrophoretic/suspended-particle devices (SPD). In terms of chromic materials, there are basically four types of chromic devices, such as gasochromic,[11] thermochromic,[12] photochromic[13] and electrochromic[14] which control the amount of solar irradiation and heat in response to external stimulus, such as gas, heat, light, or electricity. However, the application of thermochromic and photochromic devices in smart windows are limited to certain extent as their optical properties strongly depend on the temperature and light intensities and often lacking in precision control. Gasochromic switching is also a viable candidate for smart window applications. However, it requires careful control during the gas exchange processes which may not be practical in windows configuration. Moreover, the stability of the gasochromic devices requires further investigation and improvement. The mechanism of smart window based LC is based on a change in the transmittance by changing the orientation of liquid crystal molecules between two transparent conductive electrodes under a suitable voltage, which offers another choice for smart window.[15, 16] Similar to the LC-based device, the active particles in SPD are oriented randomly and absorb light in the off state, these particles align under an electric field and thus the transmittance of the device increases.[17]

Among various smart windows, electrochromic smart windows have attracted much attention and major progress has been achieved in both the practical and theoretical aspects in recent years.[18-20] Meanwhile, electrochromic smart window with novel features and extended

functionalities are of great interests.[21-23] In this review, we present the recent research advances in developing different strategies to prepare and characterize state-of-the-art electrochromic materials and high performance electrochromic smart window with multiple functionalities.

2. Electrochromic materials used for smart window

Generally, electrochromic materials can be divided into two types: anodic and cathodic chromic materials consisting of transition metal oxides (WO_3, TiO_2, MoO_3, Ta_2O_5, CeO_2, NiO, Co_3O_4, V_2O_5, *etc.*),[24-35] Prussian blue,[36] conducting polymers (polyaniline (PANI), poly(3,4-ethylenedioxythiophene) (PEDOT), polypyrrole, *etc.*),[37-43] and viologens [44-48]. Anodic electrochromic materials refer to the chromic materials whose color change from transparent state to dark or opaque state when oxidized during the anodic polarization process. Thus color change of the chromic materials from transparent state to dark or opaque state when reduced during the cathodic polarization process is the cathodic electrochormic materials. There are several key criteria to fulfill during the evaluation of the performance of the electrochromic materials. Firstly, the chromic materials should deliver high optical modulation with minimal haze in the electromagnetic spectrum of interest. Ideally, the best chromic material should deliver 100% optical modulation, that is, the chromic material can be fully transparent in bleached state and fully opaque in dark state. Secondly, the switching speed for bleaching and coloration, which can be expressed as the time required to reach 90% of the optical modulation between the steady bleached and colored states, is important. Smart window application can tolerate slower switching speed compared to display application which requires faster switching speed. Thirdly, coloration efficiency (CE), is defined as the ratio between optical modulation and the consumed charge density. It is a widely used metric to evaluate the performance of electrochromic materials. A high CE indicates that the electrochromic material exhibits a large

optical modulation with a small charge consumption. Last but not least, lifetime and cycling stability without or only minor degradation during usage must meet particular requirements (it is 30 years for smart window application). Many detailed reviews of electrochromic materials have been given in the earlier reports.[49-58]

In the past, extensive efforts were spent on the preparation of electrochromic materials to improve their electrochromic performance. Broadly, nanostructured materials with small size and large specific surface area are expected to shorten ion diffusion length, improve electrolyte accessibility and enhance the performance of electrochromic devices. The electrochromic mechanism of most electrochromic materials can be attributed to the injection/extraction of cations and electrons into/from host materials. Take WO_3 for example, the injection/extraction process can be described as:

$$WO_3 + xM^+ + xe^- \leftrightarrow M_xWO_3 \quad (1)$$

where $0 < x < 1$, and M denotes some cations, such as H^+, Li^+, K^+ and so on. The kinetics and magnitude of ion insertion and the electrochromic reaction strongly depend on the diffusion length, the diffusion coefficient of ions and the available specific surface area.[59-64] Therefore, nanostructured electrochromic material is expected to significantly reduce the diffusion length of intercalated ions, while increasing the number of accessible intercalation sites simultaneously. Moreover, the nanostructured materials can not only relieve the expansion and contraction of the host material during guest insertion and extraction, but also increase the surface-to-volume ratio. The development in past years has shown that nanostructured materials have great potential to remarkably improve the electrochromic performance. Furthermore, electrochromic film preparation with nanostructured materials are compatible with low-temperature solution deposition and low-cost processing techniques such as inkjet printing, slot die coating, roll to roll

printing, flexographic printing and lamination. This can remarkably increase production rate and reduce manufacturing costs, opening new opportunities to mass-produce smart window as in the production of newspapers or banknotes, providing affordable smart windows for universal use. Towards this aim, the following discussion is mainly to cover the recent developments in zero-dimensional (0D), one-dimensional (1D), two-dimensional (2D), three-dimensional (3D) hierarchical nanostructured and ordered macroporous electrochromic materials for advanced electrochromic devices.

2.1 0D nanostructured electrochromic materials

0D nanostructured electrochromic materials such as quantum dot, nanocrystal, nanoparticles arrays and hybrid nanoparticles have been fabricated by various strategies recently.[42, 65-73] 0D nanostructured electrochromic materials are compatible with most of the large scale film processing techniques such as inkjet printing, slot die coating, spray coating, spin coating, roll-to-roll printing, flexographic printing and lamination *etc*. Recently, we fabricated 0D WO_3 nanoparticles with sizes of 10-40 nm via facile electrodeposition method in the deposition solution containing $Na_2WO_4 \cdot 2H_2O$ on flexible silver grids/PEDOT:PSS transparent conductors as shown in **Figure 1**a.[74] The WO_3 films can change its color reversibly from transparent to dark blue with small alternating electric field. The WO_3 nanoparticles present an optical modulation of 81.9% at 633 nm, high CE value of 124.5 $cm^2\ C^{-1}$, and fast switching speed of 2.8 and 1.9 s for bleaching and coloration process, respectively (Figure 1b and c). Moreover, excellent cycling stability with retention of 79.1% of their initial transmittance modulation after 1,000 cycles is achieved (Figure 1d). Liu et al. synthesized WO_3 crystalline nanoparticles with size of 50-80 nm via "nano to nano" electrodeposition approach.[75] The deposition solution is 5 wt% nano-crystalline WO_3 dispersed in water without addition of additive. The electrodeposited

film is comprised of stacked nanoparticles, which exhibits outstanding electrochromic performance and stability including 92% optical modulation, 9 and 15 s for coloring and bleaching, sustaining 76% optical modulation after 1,000 cycles. In order to optimize the electrochromic performance, hybrid WO_3 nanoparticles can be also fabricated by electrodeposition technique.[76, 77] Ling et al. introduced one-pot sequential electrochemical deposition approach to prepare a hybrid thin film composed of multilayer poly(3,4-ethylenedioxythiophene):poly(4-styrenesulfonic acid) (PEDOT:PSS) and WO_3 nanoparticles.[78] The hybrid thin film exhibits significantly improved optical modulation and stability compared with neat PEDOT:PSS or WO_3 films. Electrodeposition technique can be used to fabricate other 0D electrochromic nanomaterials such as NiO nanoparticles[79] and Prussian blue nanoparticles [80] with ultra fast electrochromic switching speed.

Besides electrochemical deposition method, sol-gel approach is another most common method for electrochromic nanoparticles preparation.[81-83] After coating these nanoparticles on transparent conductors by inkjet printing or spray coating technique, the film exhibited large optical modulation and fast switching speed. Solvothermal is another simple and low-cost method for uniform electrochromic nanoparticles preparation. Recently, we synthesized uniform NiO nanoparticles on different substrates via solvothermal method at 200 °C for 24 h with nickel acetylacetonate dispersed in tert-butanol as precursor as shown in **Figure 2**.[84] The color of the NiO electrochromic materials changed from transparent to brown color reversibly with applied small alternating electric field. An optical modulation of 63.6% at 550 nm, a CE of 42.8 $cm^2\ C^{-1}$ at 550 nm and 5000 electrochemical cycles were achieved when the NiO nanoparticles are used for electrochromic application.

In addition, Geng's group developed tungsten oxide quantum dot with an average crystalline size of 1.6 nm synthesized via simple colloidal process.[85] After coating tungsten oxide quantum dot onto FTO glasses as the electrochromic film, excellent electrochromic performance including fast coloration/bleaching speed (within 1 s), high coloration efficiency (154 cm^2 C^{-1}) and the large optical modulation (85% at 633 nm) were achieved (**Figure 3**a-c). Milliron's group illustrated composite nanocrystals by introducing tin-doped indium oxide nanocrystals into niobium oxide glass (NbO_x), and realized a new amorphous structure as shown in Figure 3d and e.[20] This electrochromic material is capable of controlling visible light and near-infrared transmittance individually (Figure 3f). Such a dual-band film provides more choices for use in smart windows; the user can choose the bright mode which admits both NIR and visible light, the cool mode which selectively blocks NIR light or the dark mode which blocks both NIR and visible light depending on weather conditions.

2.2 1D nanostructured electrochromic materials

1D nanostructured electrochromic materials such as nanorods, nanowires, nanotubes, nanobelts and nanobundles have stimulated an increasing interest due to their importance in the development of high performance electrochromic device.[32, 86-99] They are expected to play an important role due to the enlarged surface area with nanoscale dimensions. We synthesized uniform crystalline WO_3 nanorods with diameters about 100 nm and lengths about 2 μm via a facile hydrothermal process with assistance of a capping agent NaCl in Na_2WO_4 solution as precursor (**Figure 4**).[33, 34] The growth mechanism of the 1D WO_3 nanorods can be explained according to the following reactions:

$$Na_2WO_4 + 2HCl \rightarrow H_2WO_4 + 2NaCl \quad (2)$$

$$H_2WO_4 \rightarrow WO_3 \text{ (crystal nucleus)} + H_2O \quad (3)$$

$$WO_3 \text{ (crystal nucleus)} \rightarrow WO_3 \text{ nanorods} \quad (4)$$

After coating the WO_3 nanorods onto indium tin oxide (ITO), it presented electrochromic phenomenon in both organic (lithium perchlorate ($LiClO_4$) in propylene carbonate (PC)) and aqueous (H_2SO_4) electrolytes. The film exhibited an optical modulation of 66 % under applied voltage of -3.0 V and more than 3,000 cycles in organic electrolyte, and 33.9 % of optical modulation at 632.8 nm when applying -1.0 V in H_2SO_4 aqueous electrolyte. Zhang et al fabricated hexagonal WO_3 nanowire array film on fluorine-doped tin oxide (FTO)-coated glass by optimizing the experimental conditions using $(NH_4)_2SO_4$ as capping agent.[100] The length and diameter of nanowires is about 1.5 μm and 20–40 nm, respectively. In addition, it has BET surface area of 116.5 $m^2\ g^{-1}$. The WO_3 nanowire shows an optical modulation of 58% at 633 nm and the coloration efficiency of 102.8 $cm^2\ C^{-1}$ in PC electrolyte. In addition, the length, diameter, micromorphology and degree of crystallinity of the nanowires can be tailored by adjusting some experimental conditions. Cai et al. illustrated that Ti doping can lead to significant changes in diameter, length, morphology and crystallization of the WO_3 nanowires, and affect the electrochromic performance.[25] Similar phenomenon was observed in Mo-doped WO_3 nanowires.[101] Ma et al. revealed that the urea content in precursor solution played an important role in controlling the size and shape of the WO_3 nanostructures.[102] Apart from hydrothermal method, WO_3 nanowires can be prepared by solvothermal, electrospinning, or electrophoretic deposition methods.[103-105]

1D TiO_2 materials have also been extensively studied in electrochromic applications.[106-109] However, the optical modulation of neat TiO_2 is usually small. Hence, incorporation and doping of other electrochromic materials to improve its electrochromic performance is a smart choice. Cai et al. electrodeposited WO_3 nanoparticles and PANI on the surface of TiO_2 nanorods, in

which the composite nanorod arrays exhibited remarkable enhanced electrochromic performance in terms of optical modulation, stability and ample coloration.[38, 110] The enhanced electrochromic properties are mainly attributed to the unique porous core/shell structure, which makes the ion diffusion and charge-transfer become easier. Schmuki's group illustrated that the optical modulation of TiO_2 nanotubes can be significantly improved after compositing with WO_3 electrochromic materials.[87, 111]. Vuong et al. also observed that the TiO_2/WO_3 core/shell nanowire structure could highly enhanced the optical modulation and CE due to the porous composite nanowire structure showed an improved proton intercalation capacity.[112] Yao et al. proved that after coating MoO_3 layer on TiO_2 nanotubes system, optical density can be increased over four times compared to bare TiO_2 nanotubes when the thickness of the MoO_3 coating layer was optimised.[27]

Apart from WO_3 and TiO_2, 1D V_2O_5 is another extensively studied electrochromic material which exhibits a green-blue and orange colour when applying negative and positive potentials, respectively. Xiong et al. have synthesized silver vanadium oxide and V_2O_5 nanowires with length over 30 μm and diameter about 10–20 nm by hydrothermal method.[113] The electrochromic device fabricated from the silver vanadium oxide nanowires exhibited switching time of 0.2 s from the green state to the red-brown state with optical modulation of 60%. Recently, we have fabricated 1D V_2O_5 nanoribbons by electrodeposition method.[35] The electrochromic performances of the V_2O_5 nanoribbons were enhanced by doping Ti in the V_2O_5 , resulting in higher optical modulation (51.1%), higher CE (95.7 cm^2 C^{-1}) at 415 nm and faster switching speed compared with the pure V_2O_5. To further improve the electrochromic performance, nanobelt-membrane hybrid structured V_2O_5 was prepared by hydrothermal synthesis approach.[32] Transmission electron microscopy (TEM) images revealed that the width

of the thin nanobelts was around 20–40 nm. The hybrid structured V_2O_5 displayed high optical modulation of 62% at 700 nm. The stability can be greatly enhanced with linear polyethylenimine (LPEI) surface treatment on the transparent conductor.

Patil et al. synthesized transparent 1D NiO nanorods on a conducting indium tin oxide thin film via hot-filament metal-oxide vapor deposition (**Figure 5**).[114] The film contains nanorods grown within a square micrometer, and the length and width of the nanorods are 500 nm and 100 nm, respectively (Figure 5b). Large optical modulation (about 60%), stable and reversible coloration–bleaching cycles, and fast coloration and bleaching speed as well as high coloration efficiency (43.3 cm^2 C^{-1}) were achieved by the 1D NiO nanorods. Other 1D electrochromic nanomaterials such as Co_3O_4 nanowires, and PANI nanowires with outstanding electrochromic performances can also be fabricated by various fabrication techniques. [115-117]

2.3 2D nanostructured electrochromic materials

2D nanostructured electrochromic materials such as nanosheets, nanoflakes, nanowalls and nanoplates with two dimensions outside of the nanometric size range are attracting much attention recently due to their unique shape-dependent characteristics.[31, 118-123] Recently, we fabricated porous WO_3 film with 2D flake nanostructures by novel, facile and low-cost pulsed electrochemical deposition method.[124] The reaction can be explained as follows:

$$2WO_4^{2-} + 4H_2O_2 \rightarrow W_2O_{11}^{2-} + 2OH^- + 3H_2O \quad (5)$$

$$W_2O_{11}^{2-} + (2+3x)H^+ + 3xe^- \rightarrow 2H_xWO_3 + \frac{(2+x)}{2}H_2O + \frac{8-x}{4}O_2 \quad (6)$$

$$H_xWO_3 \rightarrow WO_3 + xH^+ + xe^- \quad (7)$$

The thickness of the WO_3 flake is about 25 nm and interconnected with each other. This nanostructured WO_3 film displayed a near ideal optical modulation of 97.7% at 633 nm, fast

switching speed (6 and 2.7 s for for coloration and bleaching process), high CE of 118.3 $cm^2\ C^{-1}$, and excellent cycling stability. Wang et al. have prepared 2D crystalline WO_3 nanosheets on FTO coated glass via layer-by-layer (LBL) technique.[125] The thickness of the nanosheets is about 30 nm with lateral sizes in the range of 300–500 nm. The nanosheet film displays transmittance modulation of 48.5% at 800 nm and a CE of 32 $cm^2\ C^{-1}$. Hydrothermal is one of the facile methods to fabricate 2D WO_3 electrochromic nanomaterials. Jiao et al. synthesized WO_3 nanoplates on FTO glass by hydrothermal approach (**Figure 6**a, b).[126-128] The morphology of the 2D structured electrochromic WO_3 film can be selectively synthesized by adding different capping agents such as Na_2SO_4, $(NH_4)_2SO_4$, or CH_3COONH_4 in the precursor and both the uniformity and adhesion can be improved via a pre-coated seed layer onto the FTO substrates. The growth mechanism of the 2D WO_3 nanoplates can be described in the following reactions:

$$Na_2WO_4 + 2HCl \rightarrow H_2WO_4 + 2NaCl \quad (8)$$

$$H_2WO_4 + xH_2O_2 \rightarrow WO_3 \cdot xH_2O_2 \cdot H_2O \text{ (peroxopolytungstic acid)} \quad (9)$$

$$2WO_3 \cdot xH_2O_2 \cdot H_2O \rightarrow 2WO_3\text{(crystal nucleus)} + 2(x + 1)H_2O + xO_2 \quad (10)$$

$$WO_3\text{(crystal nucleus)} \rightarrow WO_3\text{(nanoplate)} \quad (11)$$

The nanoplate film exhibited high CE of 112.7 $cm^2\ C^{-1}$ and fast switching speed of 4.3/1.4 s for coloration and bleached process, respectively. Recently, Cai et al. illustrated that the WO_3 nanosheets can be prepared by adjusting the pH value of the precursor without using template and capping-agent (Figure 6 c, d).[129] The thickness of the WO_3 nanosheets is 10–15 nm. Large optical modulation in both visible and NIR range (62% at 633 nm, 67% at 2000 nm), fast switching speed (5.2 and 2.2 s for coloration and bleaching process, respectively), excellent cycling stability (sustaining 95.4% even after 3,000 cycles) are achieved for the WO_3 nanosheet array film.

2D structured NiO nanosheets have attracted considerable attention because of its large optical modulation range, high CE, and low material cost *etc*. Tu's group have synthesized NiO nanosheets on ITO glass by combination of chemical bath deposition (CBD) method and followed by heat-treatment process.[130] The hydroxide precursor preparation can be described in the following reactions:

$$[Ni(H_2O)_{6-x}(NH_3)_x]^{2+} + 2OH^- \rightarrow Ni(OH)_2 + (6\text{-}x)\,H_2O + xNH_3 \quad (12)$$

$$2Ni(OH)_2 + S_2O_8^{2-} \rightarrow 2NiOOH + 2SO_4^{2-} + 2H^+ \quad (13)$$

After annealing, the nickel hydroxide changed to NiO and the film was transparent. The NiO nanosheet film exhibited an optical modulation of 82% at 550 nm with switching speed of 8/10 s for coloration/bleached process and CE of 42 $cm^2\ C^{-1}$. The electrochromic performances such as switching speed, CE and stability can be further improved by incorporating with graphene or TiO_2 nanorods or doping Co element in the NiO nanosheet (**Figure 7**).[86, 131, 132] Similar 2D structured NiO nanosheets, nanowalls or nanoflakes can also be fabricated by other synthesis methods such as electrodeposition[133] and hydrothermal methods.[134, 135]

2.4 3D hierarchical nanostructured electrochromic materials

Ordered arrangement and construction of low dimensional nanomaterials as building blocks with two or more levels from the nanometer to the macroscopic scale leads to the formation of three-dimensional hierarchical nanostructures. The 0D, 1D and 2D structural elements in the 3D nanostructured material are in close contact with each other and form interconnected interfaces in repeated assemblied. 3D hierarchical nanostructured electrochromic materials including nanotree arrays, nanocluster, gyroid, urchins and nanoflowers were widely investigated due to the large specific surface area, well-interconnected pores and other superior characteristics over their bulk counterparts.[58, 136-138] Cai et al. produced a variety of 3D hierarchic nanostructured

WO_3 electrochromic materials such as nanocluster, nanotree and nanowire arrays on FTO-coated glass by solvothermal method without any template (**Figure 8**a-c).[139] The reaction process can be ascribed to alcoholysis reaction between $W(CO)_6$ and ethanol and the thickness of the obtained nanostructured array is about 1.1 μm. The nanostructured WO_3 nanotree arrays exhibited large optical modulation in visible, NIR and mid-infrared ranges such as 66.5% at 633 nm, 73.8% at 2 μm, 57.7% at 8 μm, fast switching speed of 4.6/3.6 s for coloration/bleached process, high coloration efficiency of 126 $cm^2\ C^{-1}$ at 633 nm and excellent cycling stability (maintaining optical modulation of about 80% after 4,500 cycles) (Figure 8d, e). Steiner's group have demonstrated that fabricating of V_2O_5 and NiO in a 3D periodic interconnected gyroid structure on the nanoscale length leading to remarkable improvement of electrochromic performance (**Figure** 9).[61, 140, 141] The 3D periodic interconnect gyroid structured metal oxide enhanced the ions intercalation and showed substantially enhanced electrochromic performance, such as high coloration contrast and fast switching speeds. Kim have illustrated nano-urchin structured tungsten oxide comprised of the $W_{18}O_{49}$ nano-wires added to the sphere shell fabricated by solvothermal method.[137] The nano-urchin-like electrochromic film displays fast switching speed, high CE of 132 $cm^2\ C^{-1}$, and good durability in the acidic electrolyte. Xiao et al. also fabricated similar struture of WO_3 by one-pot hydrothermal method with the assistance of Na_2SO_4, but the sphere shell is comprised of WO_3 nanosheet.[142] Na_2SO_4 acted both as stabilizer which facilitated the generation of a metastable hexagonal phase as well as structure directing agent that assisted nanosheet assembly. This hexagonal-phase WO_3 nanosheet/microflower hierarchical structure exhibited an optical modulation of 33% at 700 nm and switching speed of 90/60 s for coloration/bleached process in organic $LiClO_4$ electrolyte when applying bias of ±3.0 V. Dalavi et al. have reported that NiO can also form dandelion flower-like structure. The size

of NiO flowers is about 2–3 μm which composed of nano-flakes with an average thickness of 35–40 nm.[143] The dandelion flower-like NiO film presents an excellent electrochromic behavior such as high optical modulation of 68.09%, high CE of 88 cm^2 C^{-1} at 555 nm and fast switching speed of 5.84/4.43 s for coloration/bleached process.

2.5 3D ordered macroporous electrochromic materials

Besides the nanostructured electrochromic materials, three-dimensionally ordered macroporous (3DOM) electrochromic materials have attracted considerable attention due to their outstanding electrochromic performance. Monodispersed polystyrene (PS) latex spheres were often used as templates to prepare 3DOM structured electrochromic materials. Tu's group have prepared macroporous WO_3 and Co_3O_4 electrochomic films by using monolayer PS spheres template (**Figure 10**a, b).[144-146] All the macroporous films show connected network of close-packed microbowl arrays with average size of 600 nm after removing the PS sphere templates. The macroporous electrochromic films show superior electrochromic properties with higher CE, faster switching speed, larger optical modulation compared with the dense electrochromic film. Yuan et al. have prepared macroporous NiO film using similar template method.[147] The ordered macroporous NiO film exhibits good optical modulation of 76% at 550 nm, fast switching speed (3/6 s for coloration and bleached process), high CE of 41 cm^2 C^{-1} and good stability. Li's group also synthesized thick three-dimensionally ordered macroporous structured WO_3 and V_2O_5 electrochromic films via multilayer PS spheres template methods (Figure 10c-d).[148-150] Significant improvement in electrochromic performance is achieved by the ordered multilayer interconnected porous structure due to the porous structure which facilitates the ions diffusion.

3. Smart window preparation

3.1 Electrochromic active layer deposition

Generally, electrochromic smart windows have multilayer structure as shown in **Figure 11** which comprised of two sheets of transparent conductors, one electrochromic layer, one transparent ion conductor layer (electrolyte) and one ion-storage layer.[21] When liquid or semisolid electrolyte was used in electrochromic device, a spacer is needed between the two parallel transparent conductors to maintain the accurately defined distance of the two conductors. Each layer of the smart window must be highly transparent in the visible light at bleached state, and their refractive index must matched with each other to minimize the reflections of the window. In addition, all the layers must have excellent weathering and electrochemical stability to avoid early failure of the window during use.

Smart windows need to meet the architectural aesthetic demands and stability, and its size is larger than the usual electrochromic device. Therefore, the low-cost and large area film preparation techniques are attracting increasing attention in smart window fields. In the past, magnetron sputtering spearheaded the coating process for large area smart window film coating as it provides reasonable deposition rates (dynamic deposition rate 18 nm×m/min, mean static deposition rate 1.5 nm s^{-1}) for industrial production as well as good coating uniformities.[151-153] Today, spray coating, spin coating, printing, roll to roll techniques and combined techniques such as printing/roll to roll and sputtering/roll to roll techniques have been investigated for smart window film fabrication due to their advantages such as low-cost, high speed, great efficiency, and ease of scalability.[154] Most of these solution-processable techniques mentioned above required preparation of ink from nanostructured electrochromic materials and thus, ink formulation becomes one of the key components in evaluating the coating process. Printing techniques used in electrochromic film preparation usually include screen printing, inkjet printing, flexographic printing, slot die and rotogravure printing.

We have fabricated uniform and continuous tungsten molybdenum oxide electrochromic film from aqueous ink via a simple and low cost spray coating technique recently (**Figure 12)**.[83] The thickness of the as-prepared film is about 200 nm with a surface roughness of about 60 nm. The spray coated tungsten molybdenum oxide film displays an optical modulation of 42.9% at 632.8 nm, a CE of 36.3 cm^2 C^{-1}, switching speed of 10/7 s for coloration/bleached process and excellent stability (more than 2,000 cycles). Meanwhile, Shin et al. fabricated an electrochromic windows using p-conjugated polymers as electrochromic film and ionic liquid (IL) as the electrolyte.[155] The electrochromic film was coated onto the ITO glass by spin coating. The length of the window can reach up to 7 inchs. The electrochromic window provides a bistability (more than 90 min) at V-Off state by controlling the interfacial charge transport. It is not easy to deliver controllable thickness and low surface roughness of the large scale films with spray coating and spin coating, these techniques have limited patterns in design flexibility and typically require post coating heat treatment.

Inkjet printing is an economical manufacturing technology which can be used for fabricating electrochromic materials on all kinds of substrates and is a highly attractive technology as it offers ease of scaling-up for mass production. Moreover, inkjet printing allows deposition of electrochromic materials on a specific location as well as precise thickness control. Recently, we printed high quality electrochromic films by inkjet printing such as WO_3, NiO, TiO_2, CeO_2, PEDOT:PSS and their composite films (**Figure 13)**.[81, 156, 157] All the printed samples are uniform continuous films and do not showed any aggregation. A complementary all solid-state electrochromic device was fabricated by assembling inkjet printed WO_3 and NiO films as the electrochromic layer, the ion-storage layer, respectively, and PMMA-based gel electrolyte as the solid electrolyte. This complementary electrochromic device delivered large optical modulation

of 75.4% and high CE of 131.9 cm^2 C^{-1} at 633 nm. The NiO ion-storage layer can be replaced by passive CeO_2/TiO_2 as the counter electrode. Passive counter electrode can be used to balance the charge shuttled from the electrochromic layer and possesses high transmittance with small optical changes in the visible light wavelength during the cations insertion. The smart windows assembled by inkjet printed CeO_2/TiO_2 and WO_3/PEDOT:PSS films display an optical modulation of above 70% at 633 nm, switching speed of 12.7/15.8 s for coloration/bleached process as well as high CE of 108.9 cm^2 C^{-1} at 633 nm and excellent bistability. Moreover, large area smart window (360 cm^2) with excellent electrochromic performance can be prepared by inkjet printing as shown in **Figure 14**. The large smart window exhibits an optical modulation of 70.4% at 633 nm and switching speed of 18 and 17 s for coloration/bleached process, which delivers almost the same electrochromic performance of a small device.

3.2 Electrochromics device on flexible transparent conductors

Integration of different coating techniques for industrial scale production is an inevitable trend in various industries, and smart window is of no exception. Electrochromic materials coated on flexible substrates to fabricate flexible electrochromic devices have attracted more interests lately because of their compatibility with roll to roll technology. Flexible smart windows can be used in buildings, automobiles and airplanes *etc*. Sputtered ITO onto plastic is one way to prepare flexible electrode, but it has several limitations such as intrinsic brittleness of ITO, low scarcity of indium, and expensive processing. Therefore, possible ITO alternatives are being extensively investigated such as conducting polymers,[158] carbon-based materials [159, 160] and metal-based materials for transparent conductive electrode applications.[161-164] We produced flexible electrode by self-assembling and sintering of silver (Ag) nanoparticles on poly(ethylene terephthalate) (PET) substrate, and then coated electrochromic WO_3 layer onto the flexible electrode by inkjet printing.[81] The flexible Ag grid electrodes show a high transmittance of 82 ±

3% in the wavelength of 350−900 nm and low sheet resistance (< 5 Ω/sq). The electrochromic performance can still be maintained even after bending the flexible electrochromic films. However, the tendency of the metal-based transparent electrodes to get oxidized in both air and electrochemical reactions have limited their application in most fields. This drawback can be relieved by coating another conductive, passivation layer.[165] Recently, we have improved the stability of the Ag grid by coating PEDOT:PSS layer by spin coating.[74] The Ag grid/PEDOT:PSS hybrid film was passivated from moisture and oxygen at 65 % relative humidity at room temperature when monitored for a period of two months. After coating a layer of WO_3 on this hybrid flexible electrode using electrodeposition method, the electrochromic film possesses excellent stability during electrochemical cycling and mechanical stability. The optical modulation was maintained at 80% after 800 tensile bending cycles and 92.5% after 1,200 compressive bending cycles (**Figure 15**a-d). We further developed flexible electrode using nanocellulose paper to replace PET as the transparent substrate due to its advantages such as a ubiquitous source, biocompatibility, biodegradable nature and ability to endure large bending angles.[46, 166] Ag nanowire percolating network on transparent nanocellulose paper were realized using an innovative nanopaper-transfer method. The nanopaper electrode displays excellent flexibility and high conductivity even after repeated 200 folding cycles (Figure 15e-g). The conductive and mechanical stability of this transparent conductive nanopaper can be further enhanced by coating a layer of single-walled carbon nanotubes (SWCNTs). The SWCNTs fuse and bridge the Ag nanowires to improve the electrode conductivity while protecting and anchoring Ag nanowires to withstand external deformations. Electrochromic device constructed by the transparent conductive nanopaper has strong endurance towards deformation within large bending angles as well as excellent coloration efficiency and good stability. Besides flexible and

foldable electrochromic devices, stretchable electrochromic devices also have potential applications in displays which can be integrated in future smart windows.[167, 168] In our previous work, stretchable conductors were fabricated by embedding AgNW networks in the polydimethylsiloxane (PDMS) elastomer matrix in order to prepare the stretchable electrochromic device (Figure 15h, i).[169] After coating electrochromic WO_3 layer on the stretchable conductors, the stretchable electrochromic devices were mechanically robust and can be twisted, folded, crumpled and stretched without undergoing electrochromic degradation. The stretchable electrochromic device maintained its electrochromic functionality even under 50% strain state, shows a large optical modulation at 350 nm, fast switching speed of 1/4 s for coloration/bleached process as well as good cycling stability in the relaxed state.

There are other efforts on integration of different techniques to fabricate large scale flexible electrochromic devices. Krebs's group manufactured flexible electrochromic device by combination of flexographic printing, slot die coating and roll to roll technology as shown in **Figure 16.**[170, 171] Solid state electrochromic devices can be fabricated by sequentially stacking the layers in one direction via integrated flexographic printing and slot-die coating techniques. The flexible electrochromic devices display an optical modulation of 35%, and switching speed of 25 s between +1 V to –0.4 V. Kim's group prepared flexible ITO/Ag/ITO and ITO/Cu/ITO on PET substrate via combination of sputtering and roll to roll processes**.**[172, 173] Mechanical fatigue tests demonstrated that the multilayer electrodes have better flexibility than that of a sputtered ITO on PET substrate. Electrochromic layer coated on multilayer electrode exhibits long-term stability as well as fast switching speed for coloration and bleached process. Undoubtedly, there are many other coating techniques which can be potentially used to manufacture electrochromic devices, which are not discussed in this review.

3.3 Self-powered electrochromic smart window

Conventional smart windows consume electricity, which is generated by fossil fuels. Excessively relying on the fossil energy will result in energy crisis and environmental pollution. Renewable energy sources such as solar, wind, rain, tides and geothermal heat have been exploited in recent years to alleviate the energy crisis, environmental pollution and resources wasting. Among them, solar energy is one of the most sought-after renewable energy sources to be integrated with the smart windows. Bechinger and co-workers demonstrated self-powered electrochromic windows in 1996, introducing the term, photoelectrochromic cells (PECC).[174] The PECC device has a similar configuration with dye-sensitized solar cells. Both configurations use dye-sensitized TiO_2 nanoparticle film as the photoanode, but WO_3 electrochromic film replaced the Pt counterelectrode in PECC. Under illumination, the photoelectrons generated at the dye-sensitized TiO_2 anode move to the electrochromic WO_3 electrode *via* an external circuit, which drives the intercalation of cations in the electrolyte into the WO_3 lattice to form bluish–coloured Li*x*WO_3, resulting in an opaque device. The colored device can spontaneously bleached when the light was blocked at short circuit, however, the speed for bleached process is rather slow. PECC was further constructed using a Pt as counter electrode and adding WO_3 to the photoanode, where Pt can accelerate the bleached process without interfering the coloration process.[175, 176], Wu et al. further developed the device by integrating solar cell and PECC, resulting in photovoltachromic cell (PVCC) which can collect solar energy to stimulate chromic behavior.[177] The PVCC composed of a dye-sensitized TiO_2 photoanode and a patterned WO_3/Pt electrode as shown in **Figure 17**a. PVCC displayed faster bleaching speed at both short circuit (dark state) and open circuit (illumination state) than that of the PECC. Recently, self-powered electrochromic windows driven by dye-sensitized solar cells, InGaN/GaN solar cell and perovskite solar cells have been developed (Figure 17b, c**)**.[178-182] In these self-powered integrated systems, the solar

cells absorb sunlight and convert it into electricity to power the electrochromic windows, effectively adjusting the throughput of the sunlight and solar heat into the building by reversibly changing the windows color.

Apart from solar energy, mechanical energy can also be used to power electrochromic window for self-powered smart window systems. Wang's group designed self-powered smart window systems driven by nanogenerators.[183, 184] In their self-powered systems, nanogenerator converts ambient mechanical energy (blowing wind, raindrops) into electricity and then drives the electrochromic smart windows to change optical properties reversibly. The maximum optical modulation can reach up to 32.4% at 695 nm. Chemical energy is another viable sustainable energy for self-powered smart window systems. Wang et al. illustrated a self-powered electrochromic window which consists of a Prussian blue layer on ITO glass, and a strip of Al sheet attached on ITO glass and 3 mol l^{-1} aqueous KCl as the electrolyte (**Figure 18**).[185] Prussian blue (blue in color) can be reduced to Prussian white (colourless) by Al sheet in KCl electrolyte, leading to self-bleaching of the window. The device turned to blue color by disconnecting the Al sheet and Prussian white electrodes. The coloration and bleached process can be described via the following reactions:

$3KFe^{III}[Fe^{II}(CN)_6]$ (Prussian blue)$+3K^+ + Al = 3K_2Fe^{II}[Fe^{II}(CN)_6]$ (Prussian white) $+Al^{3+}$ (14)

$4K_2Fe^{II}[Fe^{II}(CN)_6]$ (Prussian white) $+ O_2 + 2H_2O = 4\ KFe^{III}[Fe^{II}(CN)_6]$ (Prussian blue) $+ 4K^+ + 4OH^-$

(15)

However, the bleached device recovers its blue color state by oxidation of oxygen, which requires a very long recovering time (12 hours). When adding a trace amount of strong oxidants in the electrolyte such as NaClO, H_2O_2 and $(NH_4)_2S_2O_8$, this could oxidize the Prussian white to

Prussian blue within a few minutes, speeding up the recovery process of the self-powered electrochromic window.[186, 187]

3.4 Multifunctional electrochromic smart window

The self-powered electrochromic window reviewed above offers various ways to integrate sustainable energy sources in smart window. smart windows installed on buildings can reduce energy consumption dramatically by reducing the cooling loads, heating loads or electrical lightings, as well as protecting users′ privacy. Meanwhile, reutilization of the stored energy in the electrochromic smart window is equally important in future energy solutions. The electrochromic process of the smart window is related to the insertion and extraction of ions into and out of the electrochromic film, accompanied by energy storage as both shared the same electrochemical process within the same electrolyte reservoir. Therefore, smart window becomes an energy storage device with a rational circuit design, and the stored energy can be released from smart window to drive other electronic devices. Moreover, smart windows with more novel features and more functionalities to extend their application range are of great interests.[188] Recently, we demonstrated a series of multifunctional electrochromic films including NiO, WO_3 and WO_3/PEDOT:PSS films used for multifunctional smart windows as shown in **Figure 19**.[21, 74, 84, 157] The color of the anodic NiO film changes from transparent to brown during the charging process, and the brown color fades away during the reverse discharging process (Figure 19a). Moreover, the level of stored energy in the NiO film can be visually monitored through the color change. When the NiO electrode is charged to a fully charged state at a potential of 0.5 V in a KOH electrolyte, the film displayed a dark brown color. When the electrical charge is completely consumed in reverse discharging process, the film recovers its transparent state at a potential of 0 V. For cathodic electrochromic WO_3 based film, the charging and discharging process correspond to the downward lines and the upward lines, respectively (Figure 19b). The color of

the WO_3 film changed to deep blue when it was charged to –0.7 V in H_2SO_4 elelctrolyte. When the discharge process is completed at a potential of 0 V in a reverse process, the colored WO_3 film turns to transparent state. When a multifunctional smart window was fabricated by assembling inkjet printed WO_3/PEDOT:PSS and CeO_2/TiO_2 films as the cathode and anode, respectively, and H_2SO_4 aqueous solution as the electrolyte. A dark blue colored state is observed by polarizing the smart window to 2.5 V, and the colored smart window can recover the transparent state by applying a voltage of −2.0 V (Figure 19c-e). The redox reactions in both cathode and anode can be described as follows:

$$WO_3 + xH^+ + xe^- \leftrightarrow H_xWO_3 \quad (16)$$

$$PEDOT^+ \cdot PSS^- + H^+ + e^- \leftrightarrow PEDOT^0 \cdot PSS^- \cdot H^+ \quad (17)$$

$$4CeO_2 + 4H^+ + 4e^- \leftrightarrow 2Ce_2O_3 + 2H_2O \quad (18)$$

$$TiO_2 + xH^+ + xe^- \leftrightarrow TiOOH \quad (19)$$

The smart window exhibits an optical modulation of about 70% at 633 nm during the charge and discharge process and the level of energy storage can be monitored by the visual color changes. Moreover, four smart windows (each window with size of 4.5 × 4.5 cm^2) connected in series can light up one light-emitting diode for more than two hours. Recently, other groups have also demonstrated similar multifunctional smart windows with excellent performance using inorganic and organic electrochromic materials.[117, 178, 189]

3.5 Reflective electrochromic smart window

Reflective electrochromic smart window is another type of electrochromic devices which mainly based on reversible metal (Bi, Ag, Cu, Pb, and others) deposition–dissolution.[190-197] Reflective electrochromic smart window basically consists of a pair of parallel transparent conductive electrode with electrochromic material dissolved in an electrolyte fixed between the two parallel

transparent electrodes. Reversible reflectance change originates from the electrodeposition of the metal layer on the transparent electrodes and the dissolution of metal into the electrolyte to adjust its optical state by passing electrical current across the device. Reflective electrochromic smart window has its own advantages and disadvantages when used in building. In order to reduce interior heating in summer, light reflecting electrochromic smart window is more effective than that of light absorbing electrochromic smart window as the light absorbing window itself may be heated via the absorption of sunlight. However, light reflecting electrochromic smart window will cause exterior glare which is known as light pollution. The visibility of exterior through the light reflecting electrochromic smart window might be inferior than the light absorbing windows.[198] Moreover, critical challenges of the light reflecting electrochromic smart window such as the poor stability of the mirror state and a lack of bistability in reflectance limit its widespread practical application.[199] Recently, we reported a Cu-based reversible electrochemical mirror device which offers reversible switchability between transparent, blue, and mirror states. The tri-state reversible electrochemical mirror device can be electrochemically tuned to achieve dual transmittance and reflectance modulations in a single device, which deliver more options to meet the outdoor or indoor glass transition operations.[200]

4.Outlook and future challenges

Till now, we have disscussed various nanostructured electrochromic materials, preparation process of large scale electrochromic films and different kinds of smart windows. In the market, some companies including SAGE Electrochromics Inc., View, Inc., Gentex Corporation, RavenBrick LLC, ChromoGenics AB, Asahi Glass Company, EControl-Glas, and Magna Glass & Window, Inc. are actively researching, manufacturing, and commercializing the smart windows. However, there are still some challenges that need to be tackled in the

commercialization of smart window. Suitable and low cost electrolyte systems that enable fast switching and robust electrochemical and environmental stability need further development. Previously, we have reviewed electrolytes in detail for electrochromic device applications.[201, 202] Electrolytes used in electrochromic device should meet the electrochromic requirements such as high ionic conductivity, high transparency, low volatility and robustness (chemical and electrochemical stability, thermal stability and mechanical stability) *etc*. So far, most electrochromic films were tested in liquid electrolyte including aqueous, organic or IL based electrolytes.[203-206] Among these liquid electrolyte, IL based electrolytes have attracted more and more attention due to the wide electrochemical potential window, high ionic conductivity, transference number and potential to be recycled after usage. Ho's group fabricated a self-standing and thermoplastic solid polymer electrolyte utilizing N,N,N′,N′-tetramethyl-p-phenylenediamine (TMPD), heptyl viologen ($HV(BF_4)_2$), succinonitrile (SN), and poly(vinylidene fluoride-co-hexafluoropropylene) (PVdF-HFP). Various amounts of the IL ($BMIMBF_4$) were added into the solid polymer electrolyte. Electrochromic device prepared based on this electrolyte exhibits a reversible optical modulation of 60.1% at 615 nm and a long-term stability. [207] Recently, they also synthesized an IL electrolyte (1-butyl-3-{2-oxo-2-[(2,2,6,6-tetramethylpiperidin-1-oxyl-4-yl)amino]ethyl}-1H-imidazol-3-ium tetrafluoroborate ($TILBF_4$), containing a stable radical, 2,2,6,6-tetramethyl-1-piperidinyl-oxy (TEMPO)) used for electrochromic application. An electrochromic device based on $TILBF_4$ and a poly(3,3-diethyl-3,4-dihydro-2H-thieno-[3,4-b][1,4]dioxepine) ($PProDOT\text{-}Et_2$) thin film was assembled. The device exhibits an optical modulation of 62.2% at 590 nm when being switched in the first transition, with fast switching speed of 4.0 s and 3.6 s for bleached for coloration processes, respectively. Moreover, A relatively high CE of 983.0 $cm^2\ C^{-1}$ was achieved at 590 nm and the

device maintained 98.0% of its initial optical modulation after 1000 cycles.[208] Lu's group proposed the strategy to introduce proton conduction into IL-based electrolyte. The IL-based polymer electrolytes are prepared by immersing the sulfonic acid-grafted P(VDF-HFP) electrospun mats in $BMIMBF_4$. PANI based electrochromic devices prepared based on this novel electrolyte show high optical modulation (56.2% at 650 nm) and fast switching speed (2 s and 2.5 s for coloration and bleached prcocess, respectively).[209] Meanwhile, polymeric ILs were also studied as electrochromic electrolyte. Shaplov et al. constructed an all-polymer-based organic electrochromic device using polymeric ionic liquids as ion conducting separators. The device shows fast switching speed (3 s), high CE (390 cm^2 C^{-1} at 620 nm), optical modulation up to 22%. [210] Thermo- and electro-dual responsive poly (ionic liquid) electrolytes based smart windows have been prepared via co-polymerization of *N*-isopropylacrylamide (NIPAM) with (or without) 3-butyl-1-vinyl-imidazolium bromide ionic liquid in which diallyl viologen (DAV) that were used as both the cross-linking agent and electrochromic material. [211] However, the adoption of these liquid electrolytes has certain drawbacks such as electrolyte leakage, solvent evaporation and sealing issues. Gel (semi-solid) electrolytes in electrochromic devices have also been reported, but bubbles trapped during the preparation process and weathering stability are some of the challenges that need to be addressed.[212-214] We fabricated polymer based electrolytes prepared via layer-by-layer (LbL) methods which is compatible with flexible substrates.[215, 216] The electrolyte with an ionic conductivity of 9.1×10^{-4} S/cm was obtained via LBL technology from linear polyethylenimine (LPEI), poly-(ethylene oxide) (PEO), and poly(acrylic acid) (PAA) on flexible ITO/PET substrate. The electrolyte is composed of four interbonding layers per deposition cycle combining electrostatic attraction and hydrogen bonding in the same structure. Recently, we demonstrated the electrochromic multilayer films prepared

by self-assembly of a complex polyelectrolyte via LbL method.[39] [PANI/PAA−PEI]n films exhibited a porous structure under an accelerated growth rates, leading to enhanced electrochromic properties. $[PANI/PAA−PEI]_{30}$ film displays an optical modulation of 30% at 630 nm and fast switching. A novel multilayer system was designed by alternatively packing PAA and polyethylene glycol (PEG)−α-cyclodextrin (αCD) complex via hydrogen-bonding via LbLself-assembly in our recent work.[217] The films with PAA and PEG-αCD complex as building blocks present high ionic conductivity of 2.5×10^{-5} S cm^{-1} at room temperature (52% RH), the value is almost two orders magnitude higher than that of the compared PEG/PAA films under the same conditions. The PAA and PEG-αCD complex electrolyte provides an insight for designing polymer based solid state electrolyte and its application toward solid state electrochromic smart windows. Improvements in the electrochemical performances are rather challenging, often resulted in trade-off between high energy storage density, fast switching speed and large optical modulation in the multifunctional energy storage smart window. Smart window packaging is another hard nut to crack and very few published papers divulge details. Chemically stable sealants are critical to the lifetime of an electrochromic device. Acetic silicone and DuPont™ thermoplastic Surlyn were claimed to be used as sealants in the electrochromic device encapsulation.[218-220] Cost is another key factor that prevented market penetration of smart window. The cost of present electrochromic windows in the market is at US$50 to US$100 per square foot (US$538 to US$1076 per square meter) estimated by National Renewable Energy Laboratory which prevents its widespread adoption of the electrochromic technology in the market. National Renewable Energy Laboratory further revealed that if the price of smart windows drop to US$20 per square foot, it will be attractive and cost-competitive enough for widespread adoption in residential building.[221] Moreover, extended efforts are required to

explore multifunctional smart window without interfering with the electrochromic performance and integrating them into green building systems. We believe that novel nanostructured materials, advanced large scale manufactured strategies, and rational device design will provide solutions to address these challenges. We hope that this review will promote a further rapid growth for both research and commercialization of multifunctional smart window.

Acknowledgements

This research is supported by the National Research Foundation, Prime Minister's Office, Singapore under its Campus for Research Excellence and Technological Enterprise (CREATE) programme.

Received: ((will be filled in by the editorial staff))
Revised: ((will be filled in by the editorial staff))
Published online: ((will be filled in by the editorial staff))

[1] P. Simon, Y. Gogotsi, *Nat. Mater.* **2008**, *7*, 845.
[2] Y. Gogotsi, P. Simon, *Science* **2011**, *334*, 917.
[3] C.-G. Granqvist, *Nat. Mater.* **2006**, *5*, 89.
[4] H. Khandelwal, A. P. H. J. Schenning, M. G. Debije, *Adv. Energy Mater.* **2017**, 1602209.
[5] Y. Wang, E. L. Runnerstrom, D. J. Milliron, *Annu. Rev. Chem. Biomol. Eng.* **2016**, *7*, 283.
[6] R. Baetens, B. P. Jelle, A. Gustavsen, *Sol. Energy Mater. Sol. Cells* **2010**, *94*, 87.
[7] G. A. Niklasson, C. G. Granqvist, *J. Mater. Chem.* **2007**, *17*, 127.
[8] N. N. Abu Bakar, M. Y. Hassan, H. Abdullah, H. A. Rahman, M. P. Abdullah, F. Hussin, M. Bandi, *Renew. Sustainable Energy Rev.* **2015**, *44*, 1.
[9] A. B. R. González, J. J. V. Díaz, A. J. Caamaño, M. R. Wilby, *Energ. Buildings* **2011**, *43*, 980.
[10] T. Ramesh, R. Prakash, K. K. Shukla, *Energ. Buildings* **2010**, *42*, 1592.
[11] V. Wittwer, M. Datz, J. Ell, A. Georg, W. Graf, G. Walze, *Sol. Energy Mater. Sol. Cells* **2004**, *84*, 305.
[12] M. E. A. Warwick, R. Binions, *J. Mater. Chem. A* **2014**, *2*, 3275.
[13] R. Pardo, M. Zayat, D. Levy, *Chem. Soc. Rev.* **2011**, *40*, 672.
[14] C. G. Granqvist, *Thin Solid Films* **2014**, *564*, 1.
[15] D. Jung, W. Choi, J.-Y. Park, K. B. Kim, N. Lee, Y. Seo, H. S. Kim, N. K. Kong, *Sol. Energy Mater. Sol. Cells* **2017**, *159*, 488.
[16] R. Yamaguchi, T. Takasu, *J. Soc. Inf. Disp.* **2015**, *23*, 365.
[17] D. Barrios, R. Vergaz, J. M. Sánchez-Pena, B. García-Cámara, C. G. Granqvist, G. A. Niklasson, *Sol. Energy Mater. Sol. Cells* **2015**, *143*, 613.

[18] R.-T. Wen, C. G. Granqvist, G. A. Niklasson, *Nat. Mater.* **2015**, *14*, 996.
[19] A. Llordes, Y. Wang, A. Fernandez-Martinez, P. Xiao, T. Lee, A. Poulain, O. Zandi, C. A. Saez Cabezas, G. Henkelman, D. J. Milliron, *Nat. Mater.* **2016**, *15*, 1267
[20] A. Llordes, G. Garcia, J. Gazquez, D. J. Milliron, *Nature* **2013**, *500*, 323.
[21] G. F. Cai, J. X.Wang, P. S. Lee, *Acc. Chem. Res.* **2016**, *49*, 1469.
[22] P. Yang, P. Sun, W. Mai, *Mater. Today*, **2016**, *19*, 394.
[23] Y. Huang, M. Zhu, Y. Huang, Z. Pei, H. Li, Z. Wang, Q. Xue, C. Zhi, *Adv. Mater.* **2016**, *28*, 8344.
[24] H. Zheng, J. Z. Ou, M. S. Strano, R. B. Kaner, A. Mitchell, K. Kalantar-zadeh, *Adv. Funct. Mater.* **2011**, *21*, 2175.
[25] G. F. Cai, X. L. Wang, D. Zhou, J. H. Zhang, Q. Q. Xiong, C. D. Gu, J. P. Tu, *RSC Adv.* **2013**, *3*, 6896.
[26] J.-Z. Chen, W.-Y. Ko, Y.-C. Yen, P.-H. Chen, K.-J. Lin, *ACS Nano* **2012**, *6*, 6633.
[27] D. Di Yao, M. R. Field, A. P. O'Mullane, K. Kalantar-zadeh, J. Z. Ou, *Nanoscale* **2013**, *5*, 10353.
[28] R. S. Devan, S.-Y. Gao, W.-D. Ho, J.-H. Lin, Y.-R. Ma, P. S. Patil, Y. Liou, *Appl. Phys. Lett.* **2011**, *98*, 133117.
[29]C. O. Avellaneda, M. A. C. Berton, L. O. S. Bulhões, *Sol. Energy Mater. Sol. Cells* **2008**, *92*, 240.
[30] G. F. Cai, J. P. Tu, C. D. Gu, J. H. Zhang, J. Chen, D. Zhou, S.J. Shi, X.L. Wang, *J. Mater. Chem. A* **2013**, *1*, 4286.
[31] X. H. Xia, J. P. Tu, J. Zhang, X. H. Huang, X. L. Wang, W. K. Zhang, H. Huang, *Electrochem. Commun.* **2008**, *10*, 1815.
[32] W. B. Kang, C. Y. Yan, X. Wang, C. Y. Foo, A. W. Ming Tan, K. J. Zhi Chee, P. S. Lee, *J. Mater. Chem. C* **2014**, *2*, 4727.
[33] J. Wang, E. Khoo, P. S. Lee, J. Ma, *J. Phys. Chem. C* **2009**, *113*, 9655.
[34] J. M. Wang, E. Khoo, P. S. Lee, J. Ma, *J. Phys. Chem. C* **2008**, *112*, 14306.
[35] Y. X. Lu, L. Liu, D. Mandler, P. S. Lee, *J. Mater. Chem. C* **2013**, *1*, 7380.
[36] X. Liu, A. Zhou, Y. Dou, T. Pan, M. Shao, J. Han, M. Wei, *Nanoscale* **2015**, *7*, 17088.
[37] S. Xiong, S. L. Phua, B. S. Dunn, J. Ma, X. Lu, *Chem. Mater.* **2009**, *22*, 255.
[38] G. F. Cai, J.P. Tu, D. Zhou, J. H. Zhang, Q. Q. Xiong, X. Y. Zhao, X. L. Wang, C. D. Gu, *J. Phys. Chem. C* **2013**, *117*, 15967.
[39] M. Q. Cui, W. S. Ng, X. Wang, P. Darmawan, P. S. Lee, *Adv. Funct. Mater.* **2015**, *25*, 401.
[40] S. So, H. W. M. Fung, K. Kartub, A. M. Maley, R. M. Corn, *J. Phys. Chem. Lett.* **2017**, *8*, 576.
[41] S. Ahmad, S. Sen Gursoy, S. Kazim, A. Uygun, *Sol. Energy Mater. Sol. Cells* **2012**, *99*, 95.
[42] H. Ling, G. Ding, D. Mandler, P. S. Lee, J. Xu, X. Lu, *Chem. Commun.* **2016**, *52*, 9379.
[43] D. Zhou, B.Y. Che, X.H. Lu, *J. Mater. Chem. C* **2017**, *5*, 1758.
[44] Y. Alesanco, J. Palenzuela, A. Viñuales, G. Cabañero, H. J. Grande, I. Odriozola, *ChemElectroChem* **2015**, *2*, 218.
[45] H. C. Moon, T. P. Lodge, C. D. Frisbie, *Chem. Mater.* **2015**, *27*, 1420.
[46] W. Kang, M.-F. Lin, J. Chen, P. S. Lee, *Small* **2016**, *46*, 6370.
[47] D. Weng, Y. Shi, J. Zheng, C. Xu, *Org. Electron.* **2016**, *34*, 139.
[48] S.-Y. Kao, H.-C. Lu, C.-W. Kung, H.-W. Chen, T.-H. Chang, K.-C. Ho, *ACS Appl. Mater. Interfaces* **2016**, *8*, 4175.
[49] C. G. Granqvist, *Sol. Energy Mater. Sol. Cells* **2000**, *60*, 201.

[50] J. M. Wang, X. W. Sun, Z. Jiao, *Materials* **2010**, *3*, 5029.
[51] S. K. Deb, *Sol. Energy Mater. Sol. Cells* **2008**, *92*, 245.
[52] C. G. Granqvist, *Sol. Energy Mater. Sol. Cells* **2012**, *99*, 1.
[53] C. G. Granqvist, *J. Eur. Ceram. Soc.* **2005**, *25*, 2907.
[54] D. Zhou, D. Xie, X. Xia, X. Wang, C. Gu, J. Tu, *Sci. China. Chem.* **2017**, *60*, 3.
[55] Z. Tong, Y. Tian, H. Zhang, X. Li, J. Ji, H. Qu, N. Li, J. Zhao, Y. Li, *Sci. China. Chem.* **2017**, *60*, 13.
[56] D. Ma, J. Wang, *Sci. China. Chem.* **2017**, *60*, 54.
[57] R. J. Mortimer, *Chem. Soc. Rev.* **1997**, *26*, 147.
[58] R. J. Mortimer, *Annu. Rev. Mater.* **2011**, *41*, 241.
[59] A. E. Aliev, H. W. Shin, *Solid State Ionics* **2002**, *154–155*, 425.
[60] S. H. Baeck, K. S. Choi, T. F. Jaramillo, G. D. Stucky, E. W. McFarland, *Adv. Mater.* **2003**, *15*, 1269.
[61] M. R. J. Scherer, L. Li, P. M. S. Cunha, O. A. Scherman, U. Steiner, *Adv. Mater.* **2012**, *24*, 1217.
[62] S. H. Lee, R. Deshpande, P. A. Parilla, K. M. Jones, B. To, A. H. Mahan, A. C. Dillon, *Adv. Mater.* **2006**, *18*, 763.
[63] H. Li, G. Shi, H. Wang, Q. Zhang, Y. Li, *J. Mater. Chem. A* **2014**, *2*, 11305.
[64] J. N. Tiwari, R. N. Tiwari, K. S. Kim, *Prog. Mater Sci.* **2012**, *57*, 724.
[65]S. Bhandari, M. Deepa, S. N. Sharma, A. G. Joshi, A. K. Srivastava, R. Kant, *J. Phys. Chem. C* **2010**, *114*, 14606.
[66] G. Garcia, R. Buonsanti, E. L. Runnerstrom, R. J. Mendelsberg, A. Llordes, A. Anders, T. J. Richardson, D. J. Milliron, *Nano Lett.* **2011**, *11*, 4415.
[67] J. Kim, G. K. Ong, Y. Wang, G. LeBlanc, T. E. Williams, T. M. Mattox, B. A. Helms, D. J. Milliron, *Nano Lett.* **2015**, *15*, 5574.
[68] X. Chang, S. Sun, L. Dong, Y. Dong, Y. Yin, *RSC Adv.* **2014**, *4*, 8994.
[69] J. Zhu, S. Wei, M. Alexander, Jr., T. D. Dang, T. C. Ho, Z. Guo, *Adv. Funct. Mater.* **2010**, *20*, 3076.
[70] S. H. Baeck, T. Jaramillo, G. D. Stucky, E. W. McFarland, *Nano Lett.* **2002**, *2*, 831.
[71] C. Costa, C. Pinheiro, I. Henriques, C. A. T. Laia, *ACS Appl. Mater. Interfaces* **2012**, *4*, 1330.
[72] M. Epifani, E. Comini, R. Díaz, T. Andreu, A. Genç, J. Arbiol, P. Siciliano, G. Faglia, J. R. Morante, *ACS Appl. Mater. Interfaces* **2014**, *6*, 16808.
[73] N. Soultanidis, W. Zhou, C. J. Kiely, M. S. Wong, *Langmuir* **2012**, *28*, 17771.
[74] G. F. Cai, P. Darmawan, M. Q. Cui, J. X. Wang, J .W. Chen, S. Magdassi, P. S. Lee, *Adv. Energy Mater.* **2016**, *6*, 1501882.
[75] L. Liu, M. Layani, S. Yellinek, A. Kamyshny, H. Ling, P. S. Lee, S. Magdassi, D. Mandler, *J. Mater. Chem. A* **2014**, *2*, 16224.
[76] C. P. Fu, C. Foo, P. S. Lee, *Electrochim. Acta* **2014**, *117*, 139.
[77] H. Ling, L. Liu, P. S. Lee, D. Mandler, X. Lu, *Electrochim. Acta* **2015**, *174*, 57.
[78] H. Ling, J. Lu, S. Phua, H. Liu, L. Liu, Y. Huang, D. Mandler, P. S. Lee, X. Lu, *J. Mater. Chem. A* **2014**, *2*, 2708.
[79] G. F. Cai, C. D. Gu, J. Zhang, P. C. Liu, X. L. Wang, Y. H. You, J. P. Tu, *Electrochim. Acta* **2013**, *87*, 341.
[80] T.-C. Liao, W.-H. Chen, H.-Y. Liao, L.-C. Chen, *Sol. Energy Mater. Sol. Cells* **2016**, *145*, Part 1, 26.

[81] M. Layani, P. Darmawan, W. L. Foo, L. Liu, A. Kamyshny, D. Mandler, S. Magdassi, P. S. Lee, *Nanoscale* **2014**, *6*, 4572.
[82] C. Costa, C. Pinheiro, I. Henriques, C. A. T. Laia, *ACS Appl. Mater. Interfaces* **2012**, *4*, 5266.
[83] H. Z. Li, J. W. Chen, M. Q. Cui, G. F. Cai, A. L.-S. Eh, P. S. Lee, H. Z. Wang, Q. H. Zhang, Y. G. Li, *J. Mater. Chem. C* **2016**, *4*, 33.
[84] G. F. Cai, X. Wang, M.Q Cui, P. Darmawan, J. Wang, A. L.-S. Eh, P. S. Lee, *Nano Energy* **2015**, *12*, 258.
[85] S. Cong, Y. Tian, Q. Li, Z. Zhao, F. Geng, *Adv. Mater.* **2014**, *26*, 4260.
[86] G.F. Cai, J.P. Tu, D. Zhou, L. Li, J.H. Zhang, X.L. Wang, C.D. Gu, *J. Phys. Chem. C* **2014**, *118*, 6690.
[87] Y.-C. Nah, A. Ghicov, D. Kim, S. Berger, P. Schmuki, *J. Am. Chem. Soc.* **2008**, *130*, 16154.
[88] S. Vankova, S. Zanarini, J. Amici, F. Camara, R. Arletti, S. Bodoardo, N. Penazzi, *Nanoscale* **2015**, *7*, 7174.
[89] J.-W. Liu, J. Zheng, J.-L. Wang, J. Xu, H.-H. Li, S.-H. Yu, *Nano Lett.* **2013**, *13*, 3589.
[90] X. W. Sun, J. X. Wang, *Nano Lett.* **2008**, *8*, 1884.
[91] E. Khoo, P. S. Lee, J. Ma, *J. Eur. Ceram. Soc.* **2010**, *30*, 1139.
[92] S. J. Yoo, Y. H. Jung, J. W. Lim, H. G. Choi, D. K. Kim, Y.-E. Sung, *Sol. Energy Mater. Sol. Cells* **2008**, *92*, 179.
[93] J. Thangala, S. Vaddiraju, R. Bogale, R. Thurman, T. Powers, B. Deb, M. K. Sunkara, *Small* **2007**, *3*, 890.
[94] J. Su, X. Feng, J. D. Sloppy, L. Guo, C. A. Grimes, *Nano Lett.* **2010**, *11*, 203.
[95] H. Chung Jung, H. Yi Hsuan, C. Chih Hao, L. Pang, T. Tseung Yuen, *IEEE Trans. Compon. Packag. Technol.* **2014**, *4*, 831.
[96] K. Qi, J. Wei, M. Sun, Q. Huang, X. Li, Z. Xu, W. Wang, X. Bai, *Angew. Chem. Int. Ed.* **2015**, *54*, 1 – 5.
[97] F. Zheng, M. Guo, M. Zhang, *Crystengcomm* **2013**, *15*, 277.
[98] F. Zheng, M. Zhang, M. Guo, *Thin Solid Films* **2013**, *534*, 45.
[99] J. Zhou, Y. Wei, G. Luo, J. Zheng, C. Xu, *J. Mater. Chem.C* **2016**, *4*, 1613.
[100] J. Zhang, J.P. Tu, X.H. Xia, X.L. Wang, C.D. Gu, *J. Mater. Chem.* **2011**, *21*, 5492.
[101] D. Zhou, F. Shi, D. Xie, D. H. Wang, X. H. Xia, X. L. Wang, C. D. Gu, J. P. Tu, *J. Colloid Interface Sci.* **2016**, *465*, 112.
[102] D. Ma, G. Shi, H. Wang, Q. Zhang, Y. Li, *J. Mater. Chem. A* **2013**, *1*, 684.
[103] H.-S. Shim, J. W. Kim, Y.-E. Sung, W. B. Kim, *Sol. Energy Mater. Sol. Cells* **2009**, *93*, 2062.
[104] H. G. Choi, Y. H. Jung, D. K. Kim, *J. Am. Ceram. Soc.* **2005**, *88*, 1684.
[105] B. Moshofsky, T. Mokari, *J. Mater. Chem. C* **2014**, *2*, 3556.
[106] A. Ghicov, H. Tsuchiya, R. Hahn, J. M. Macak, A. G. Muñoz, P. Schmuki, *Electrochem. Commun.* **2006**, *8*, 528.
[107] S. Liu, X. Zhang, P. Sun, C. Wang, Y. Wei, Y. Liu, *J. Mater. Chem. C* **2014**, *2*, 7891.
[108] P.F. Qiang, Z.W. Chen, P.H. Yang, X. Cai, S.Z. Tan, P.Y. Liu., W.J. Mai, *Nanotechnology* **2013**, *24*, 435403.
[109] R. A. Patil, R. S. Devan, Y. Liou, Y.-R. Ma, *Sol. Energy Mater. Sol. Cells* **2016**, *147*, 240.
[110] G. F. Cai, D. Zhou, Q. Q. Xiong, J. H. Zhang, X. L. Wang, C. D. Gu, J. P. Tu, *Sol. Energy Mater. Sol. Cells* **2013**, *117*, 231.

[111] A. Benoit, I. Paramasivam, Y. C. Nah, P. Roy, P. Schmuki, *Electrochem. Commun.* **2009**, *11*, 728.
[112] N. M. Vuong, D. Kim, H. Kim, *J. Mater. Chem.C* **2013**, *1*, 3399.
[113] C. Xiong, A. E. Aliev, B. Gnade, K. J. Balkus, *ACS Nano* **2008**, *2*, 293.
[114] R. A. Patil, R. S. Devan, J.-H. Lin, Y.-R. Ma, P. S. Patil, Y. Liou, *Sol. Energy Mater. Sol. Cells* **2013**, *112*, 91.
[115] X. H. Xia, J. P. Tu, J. Zhang, J. Y. Xiang, X. L. Wang, X. B. Zhao, *Sol. Energy Mater. Sol. Cells* **2010**, *94*, 386.
[116] G. F. Cai, J. P. Tu, D. Zhou, J. H. Zhang, X. L. Wang, C. D. Gu, *Sol. Energy Mater. Sol. Cells* **2014**, *122*, 51.
[117] K. Wang, H. Wu, Y. Meng, Y. Zhang, Z. Wei, *Energy Environ. Sci.* **2012**, *5*, 8384.
[118] H. Li, J. Wang, G. Shi, H. Wang, Q. Zhang, Y. Li, *RSC Adv.* **2015**, *5*, 196.
[119] C. Y. Ng, K. Abdul Razak, Z. Lockman, *Electrochim. Acta* **2015**, *178*, 673.
[120] X. H. Xia, J. P. Tu, J. Zhang, X. L. Wang, W. K. Zhang, H. Huang, *Electrochim. Acta* **2008**, *53*, 5721.
[121] L. Liang, J. Zhang, Y. Zhou, J. Xie, X. Zhang, M. Guan, B. Pan, Y. Xie, *Sci. Rep.* **2013**, *3*.
[122] D. Ma, H. Wang, Q. Zhang, Y. Li, *J. Mater. Chem.* **2012**, *22*, 16633.
[123] X. Zhang, Y. Zhang, B. Zhao, S. Lu, H. Wang, J. Liu, H. Yan, *RSC Adv.* **2015**, *5*, 101487.
[124] G. F. Cai, M. Q. Cui, V. Kumar, P. Darmawan, J. X. Wang, X. Wang, A. Lee-Sie Eh, K. Qian, P. S. Lee, *Chem. Sci.***2016**, *7*, 1373.
[125] K. Wang, P. Zeng, J. Zhai, Q. Liu, *Electrochem. Commun.* **2013**, *26*, 5.
[126] Z. Jiao, X. Wang, J. Wang, L. Ke, H. V. Demir, T. W. Koh, X. W. Sun, *Chem. Commun.* **2012**, *48*, 365.
[127] Z. H. Jiao, X. W. Sun, J. M. Wang, L. Ke, H. V. Demir, *J. Phys. D. Appl. Phys.* **2010**, *43*, 285501.
[128] Z. H. Jiao, J. M. Wang, L. Ke, X. W. Sun, H. V. Demir, *ACS Appl. Mater. Interfaces* **2011**, *3*, 229.
[129] G. F. Cai, J. P. Tu, D. Zhou, L. Li, J. H. Zhang, X. L. Wang, C.D. Gu, *CrystEngComm* **2014**, *16*, 6866.
[130] X. H. Xia, J. P. Tu, J. Zhang, X. L. Wang, W. K. Zhang, H. Huang, *Sol. Energy Mater. Sol. Cells* **2008**, *92*, 628.
[131] G. F. Cai, J. P. Tu, J. Zhang, Y. J. Mai, Y. Lu, C. D. Gu, X. L. Wang, *Nanoscale* **2012**, *4*, 5724.
[132] J. H. Zhang, G. F. Cai, D. Zhou, H. Tang, X.L. Wang, C.D. Gu, J. P. Tu, *J. Mater. Chem. C* **2014**, *2*, 7013.
[133] M. S. Wu, C. H. Yang, *Appl. Phys. Lett.* **2007**, *91*, 033109.
[134] D. Ma, G. Shi, H. Wang, Q. Zhang, Y. Li, *Nanoscale* **2013**, *5*, 4808.
[135] F. Cao, G. X. Pan, X. H. Xia, P. S. Tang, H. F. Chen, *Electrochim. Acta* **2013**, *111*, 86.
[136] T. Brezesinski, D. Fattakhova Rohlfing, S. Sallard, M. Antonietti, B. M. Smarsly, *Small* **2006**, *2*, 1203.
[137] D.-H. Kim, *Sol. Energy Mater. Sol. Cells* **2012**, *107*, 81.
[138] J. Zhang, X. L. Wang, X. H. Xia, C. D. Gu, J. P. Tu, *Sol. Energy Mater. Sol. Cells* **2011**, *95*, 2107.
[139] G. F. Cai, J. P. Tu, D. Zhou, X. L. Wang, C. D. Gu, *Sol. Energy Mater. Sol. Cells* **2014**, *124*, 103.
[140] M. R. J. Scherer, U. Steiner, *Nano Lett.* **2012**, *13*, 3005.

[141] D. Wei, M. R. J. Scherer, C. Bower, P. Andrew, T. Ryhänen, U. Steiner, *Nano Lett.* **2012**, *12*, 1857.
[142] W. Xiao, W. Liu, X. Mao, H. Zhu, D. Wang, *J. Mater. Chem. A* **2013**, *1*, 1261.
[143] D. S. Dalavi, R. S. Devan, R. S. Patil, Y.-R. Ma, M.-G. Kang, J.-H. Kim, P. S. Patil, *J. Mater. Chem. A* **2013**, *1*, 1035.
[144] X. H. Xia, J. P. Tu, J. Zhang, X. H. Huang, X. L. Wang, X. B. Zhao, *Electrochim. Acta* **2010**, *55*, 989.
[145] X. H. Xia, J. P. Tu, J. Zhang, J. Y. Xiang, X. L. Wang, X. B. Zhao, *ACS Appl. Mater. Interfaces* **2009**, *2*, 186.
[146] J. Zhang, J. P. Tu, G. F. Cai, G. H. Du, X. L. Wang, P. C. Liu, Electrochim. Acta **2013**, *99*, 1.
[147] Y. F. Yuan, X. H. Xia, J. B. Wu, Y. B. Chen, J. L. Yang, S. Y. Guo, *Electrochim. Acta* **2011**, *56*, 1208.
[148] L. Yang, D. Ge, J. Zhao, Y. Ding, X. Kong, Y. Li, *Sol. Energy Mater. Sol. Cells* **2012**, *100*, 251.
[149] Z. Tong, J. Hao, K. Zhang, J. Zhao, B.-L. Su, Y. Li, *J. Mater. Chem. C* **2014**, *2*, 3651.
[150] Z. Tong, X. Zhang, H. Lv, N. Li, H. Qu, J. Zhao, Y. Li, X.-Y. Liu, *Adv. Mater. Interfaces* **2015**, *2*, 1500230.
[151] G. Bräuer, *Surf. Coat. Technol.* **1999**, *112*, 358.
[152] A. Pennisi, F. Simone, G. Barletta, G. Di Marco, M. Lanza, *Electrochim. Acta* **1999**, *44*, 3237.
[153] I. D. Brotherston, Z. Cao, G. Thomas, P. Weglicki, J. R. Owen, *Sol. Energy Mater. Sol. Cells* **1995**, *39*, 257.
[154] P. S. Lee, G. F. Cai, A. L.-S. Eh, P. Darmawan, in *Nanomaterials for 2D and 3D Printing*, Wiley-VCH Verlag GmbH & Co. KGaA, **2017**, 317.
[155] H. Shin, S. Seo, C. Park, J. Na, M. Han, E. Kim, *Energy Environ. Sci.* **2016**, *9*, 117.
[156] G. F. Cai, P. Darmawan, M.Q. Cui, J.W. Chen, X. Wang, A. L.-S. Eh, S. Magdassi, P. S. Lee, *Nanoscale* **2016**, *8*, 348.
[157] G. F. Cai, P. Darmawan, X. Cheng, P. S. Lee, Adv. Energy Mater. **2017**, 1602598.
[158] S. Shin, M. Yang, L. J. Guo, H. Youn, *Small* **2013**, *9*, 4036.
[159] H. Peng, *J. Am. Chem. Soc.* **2008**, *130*, 42.
[160] K. S. Kim, Y. Zhao, H. Jang, S. Y. Lee, J. M. Kim, K. S. Kim, J.-H. Ahn, P. Kim, J.-Y. Choi, B. H. Hong, *Nature* **2009**, *457*, 706.
[161] Y. Jin, L. Li, Y. Cheng, L. Kong, Q. Pei, F. Xiao, *Adv. Funct. Mater.* **2015**, *25*, 1581.
[162] M. Layani, S. Magdassi, *J. Mater. Chem.* **2011**, *21*, 15378.
[163] M. Layani, A. Kamyshny, S. Magdassi, *Nanoscale* **2014**, *6*, 5581.
[164] S. Magdassi, M. Grouchko, O. Berezin, A. Kamyshny, *ACS Nano* **2010**, *4*, 1943.
[165] B. Deng, P.-C. Hsu, G. Chen, B. N. Chandrashekar, L. Liao, Z. Ayitimuda, J. Wu, Y. Guo, L. Lin, Y. Zhou, M. Aisijiang, Q. Xie, Y. Cui, Z. Liu, H. Peng, *Nano Lett.* **2015**, *15*, 4206.
[166] W. Kang, C. Yan, C. Y. Foo, P. S. Lee, *Adv. Funct. Mater.* **2015**, *25*, 4203.
[167] H.-H. Chou, A. Nguyen, A. Chortos, J. W. F. To, C. Lu, J. Mei, T. Kurosawa, W.-G. Bae, J. B. H. Tok, Z. Bao, *Nat. Commun.* **2015**, 6, 8011.
[168] H.-S. Liu, B.-C. Pan, G.-S. Liou, *Nanoscale* **2017**, *9*, 2633.
[169] C. Yan, W. Kang, J. Wang, M. Cui, X. Wang, C. Y. Foo, K. J. Chee, P. S. Lee, *ACS Nano* **2013**, *8*, 316.
[170] J. Jensen, F. C. Krebs, *Adv. Mater.* **2014**, *26*, 7231.

[171] R. R. Søndergaard, M. Hösel, M. Jørgensen, F. C. Krebs, *J. Polym. Sci., Part B: Polym. Phys.* **2013**, *51*, 132.
[172] T.-H. Kim, S.-H. Park, D.-H. Kim, Y.-C. Nah, H.-K. Kim, *Sol. Energy Mater. Sol. Cells* **2017**, *160*, 203.
[173] S.-H. Park, S.-M. Lee, E.-H. Ko, T.-H. Kim, Y.-C. Nah, S.-J. Lee, J. H. Lee, H.-K. Kim, *Sci. Rep.* **2016**, *6*, 33868.
[174] C. Bechinger, S. Ferrere, A. Zaban, J. Sprague, B. A. Gregg, *Nature* **1996**, *383*, 608.
[175] U. O. Krašovec, A. Georg, A. Georg, V. Wittwer, J. Luther, M. Topič, *Sol. Energy Mater. Sol. Cells* **2004**, *84*, 369.
[176] A. Georg, A. Georg, U. Opara Krašovec, *Thin Solid Films* **2006**, *502*, 246.
[177] J.-J. Wu, M.-D. Hsieh, W.-P. Liao, W.-T. Wu, J.-S. Chen, *ACS Nano* **2009**, *3*, 2297.
[178] Z. Xie, X. Jin, G. Chen, J. Xu, D. Chen, G. Shen, *Chem. Commun.* **2014**, *50*, 608.
[179] C.-C. Wu, J.-C. Liou, C.-C. Diao, *Chem. Commun.* **2015**, *51*, 12625.
[180] X. Xia, Z. Ku, D. Zhou, Y. Zhong, Y. Zhang, Y. Wang, M. J. Huang, J. Tu, H. J. Fan, *Mater. Horiz.* **2016**, *3*, 588.
[181] A. Cannavale, G. E. Eperon, P. Cossari, A. Abate, H. J. Snaith, G. Gigli, *Energy Environ. Sci.* **2015**, *8*, 1578.
[182] F. Zhou, Z. Ren, Y. Zhao, X. Shen, A. Wang, Y. Y. Li, C. Surya, Y. Chai, *ACS Nano* **2016**, *10*, 5900.
[183] X. Yang, G. Zhu, S. Wang, R. Zhang, L. Lin, W. Wu, Z. L. Wang, *Energy Environ. Sci.* **2012**, *5*, 9462.
[184] M.-H. Yeh, L. Lin, P.-K. Yang, Z. L. Wang, *ACS Nano* **2015**, *9*, 4757.
[185] J. Wang, L. Zhang, L. Yu, Z. Jiao, H. Xie, X. W. Lou, X. Wei Sun, *Nat. Commun.* **2014**, *5*.
[186] H. Zhang, Y. Yu, L. Zhang, Y. Zhai, S. Dong, *Chem.Sci.* **2016**, *7*, 6721.
[187] J. Zhao, Y. Tian, Z. Wang, S. Cong, D. Zhou, Q. Zhang, M. Yang, W. Zhang, F. Geng, Z. Zhao, *Angew. Chem. Int. Ed.* **2016**, *55*, 7161.
[188] V. Kumar, S. Park, K. Parida, V. Bhavanasi, P. S. Lee, *Mater. Today Energy* **2017**, *4*, 41.
[189] P. Yang, P. Sun, Z. Chai, L. Huang, X. Cai, S. Tan, J. Song, W. Mai, *Angew. Chem. Int. Ed.* **2014**, *53*, 11935.
[190] M. R. S. Oliveira, D. A. A. Mello, E. A. Ponzio, S. C. de Oliveira, *Electrochim. Acta* **2010**, *55*, 3756.
[191] D. A. A. de Mello, M. R. S. Oliveira, L. C. S. de Oliveira, S. C. de Oliveira, *Sol. Energy Mater. Sol. Cells* **2012**, *103*, 17.
[192] M. Nakashima, T. Ebine, M. Shishikura, K. Hoshino, K. Kawai, K. Hatsusaka, *ACS Appl. Mater. Interfaces* **2010**, *2*, 1471.
[193] T. J. Richardson, *Solid State Ionics* **2003**, *165*, 305.
[194] C. O. Avellaneda, M. A. Napolitano, E. K. Kaibara, L. O. S. Bulhões, *Electrochim. Acta* **2005**, *50*, 1317.
[195] B. M. Howard, J. P. Ziegler, *Sol. Energy Mater. Sol. Cells* **1995**, *39*, 309.
[196] T.-Y. Kim, *J. Inf. Disp.* **2014**, *15*, 13.
[197] K. R. Jeong, I. Lee, J. Y. Park, C. S. Choi, S.-H. Cho, J.-L. Lee, *NPG Asia Mater.* **2017**, *9*, e362.
[198] S. Araki, K. Nakamura, K. Kobayashi, A. Tsuboi, N. Kobayashi, *Adv. Mater.* **2012**, *24*, OP122.
[199] C. Park, S. Seo, H. Shin, B. D. Sarwade, J. Na, E. Kim, *Chem. Sci.* **2015**, *6*, 596.
[200] A. L.-S. Eh, M.-F. Lin, M.Q. Cui, G. F. Cai, P. S. Lee, *J. Mater. Chem. C* **2017**, *5*, 6547.

[201] A. L.-S. Eh, X. Lu, P. S. Lee, in *Electrochromic Materials and Devices*, Wiley-VCH Verlag GmbH & Co. KGaA, **2013**, 289.
[202] V. K. Thakur, G. Ding, J. Ma, P. S. Lee, X. Lu, *Adv. Mater.* **2012**, *24*, 4071.
[203] J. Zhang, J.P. Tu, G.H. Du, Z.M. Dong, Y.S. Wu, L. Chang, D. Xie, G.F. Cai, X.L. Wang, *Sol. Energy Mater. Sol. Cells* **2013**, *114*, 31.
[204] Y. Wei, J. Zhou, J. Zheng, C. Xu, *Electrochim. Acta* **2015**, *166*, 277.
[205] H. Cruz, N. Jordao, L. C. Branco, *Green Chem.* **2017**, *19*, 1653.
[206] D. Zhou, R. Zhou, C. Chen, W.-A. Yee, J. Kong, G. Ding, X. Lu, *J. Phys. Chem. B* **2013**, *117*, 7783.
[207] T.-H. Chang, C.-W. Hu, S.-Y. Kao, C.-W. Kung, H.-W. Chen, K.-C. Ho, *Sol. Energy Mater. Sol. Cells* **2015**, *143*, 606.
[208] M.-S. Fan, C.-P. Lee, R. Vittal, K.-C. Ho, *Sol. Energy Mater. Sol. Cells* **2017**, *166*, 61.
[209] R. Zhou, W. Liu, Y. W. Leong, J. Xu, X. Lu, *ACS Appl. Mater. Interfaces* 2015, 7, 16548.
[210] A. S. Shaplov, D. O. Ponkratov, P.-H. Aubert, E. I. Lozinskaya, C. Plesse, F. Vidal, Y. S. Vygodskii, *Chem. Commun.* **2014**, *50*, 3191.
[211] F. Chen, Y. Ren, J. Guo, F. Yan, *Chem. Commun*. **2017**, *53*, 1595.
[212] S. A. Agnihotry, P. Pradeep, S. S. Sekhon, *Electrochim. Acta* **1999**, *44*, 3121.
[213] F. L. Souza, M. A. Aegerter, E. R. Leite, *Electrochim. Acta* **2007**, *53*, 1635.
[214] Y. T. Chun, M. Neeves, Q. Smithwick, F. Placido, D. Chu, *Appl. Phys. Lett.* **2014**, *105*.
[215] C. A. Nguyen, S. Xiong, J. Ma, X. Lu, P. S. Lee, *Phys. Chem. Chem. Phys.* **2011**, *13*, 13319.
[216] C. A. Nguyen, A. A. Argun, P. T. Hammond, X. Lu, P. S. Lee, *Chem. Mater.* **2011**, *23*, 2142.
[217] M. Q. Cui, P. S. Lee, *Chem. Mater.* **2016**, *28*, 2934.
[218] E. Syrrakou, S. Papaefthimiou, P. Yianoulis, *Sol. Energy Mater. Sol. Cells* **2005**, *85*, 205.
[219] H. Pettersson, T. Gruszecki, L.-H. Johansson, M. O. M. Edwards, A. Hagfeldt, T. Matuszczyk, *Displays* **2004**, *25*, 223.
[220] H. J. Byker, *Electrochim. Acta* **2001**, *46*, 2015.
[221] D. R. Roberts, Preliminary Assessment of the Energy Saving Potential of Electrochromic Windows in Residential Buildings, *Technical Report NREL*, TP-550-469162009.

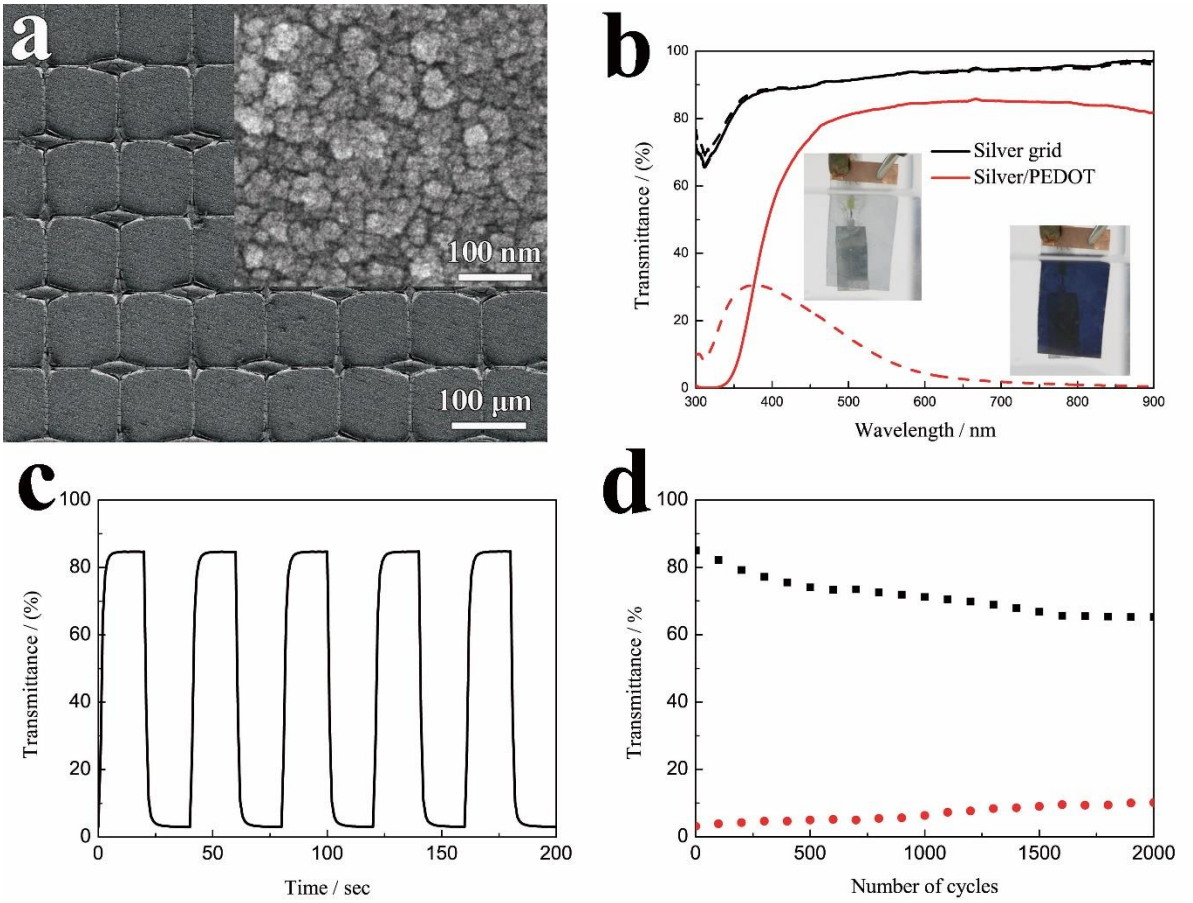

Figure 1. (a) SEM images of the of WO_3 nanoparticles electrodeposited on the flexible silver grid/PEDOT:PSS hybrid substrate. (b) Transmittance spectra of WO_3 nanoparticles deposited on the flexible pristine silver grid and the silver grid/PEDOT:PSS hybrid substrates at the colored and bleached states in the wavelength range of 300 to 900 nm. (c) Corresponding in situ optical changes of WO_3 nanoparticles on silver grid/PEDOT:PSS substrate at 633 nm. (d) Evolution of the cycling performance of WO_3 nanoparticles on the flexible silver grid/PEDOT:PSS hybrid substrate tested in 0.5 M H_2SO_4. (a-d) Reproduced with permission.[74] Copyright 2016, Wiley-VCH.

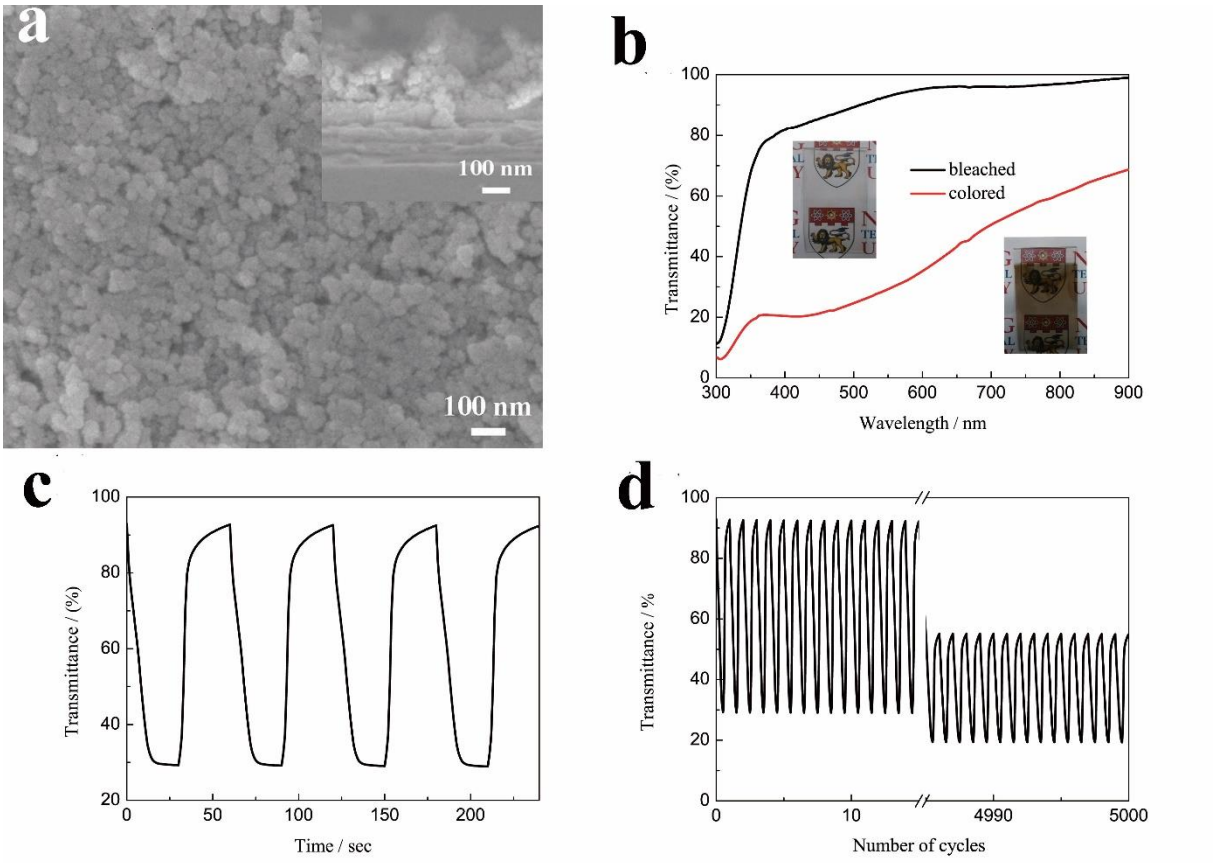

Figure 2. (a) The surface and cross-section SEM micrographs of the NiO nanoparticles growing on ITO glass with the assistance of NiO seed layer. (b) Transmittance spectra of the NiO nanoparticles with seed layer on ITO glass at the bleached and colored states (the digital photos of NiO film layer at bleached state and colored state are presented in inset). (c) In situ optical changes of the electrochromic NiO films monitored at 550 nm for 30 s per step. (d) Evolution of the cycling performance of the NiO nanoparticles film tested in 1 M KOH. (a-d) Reproduced with permission.[84] Copyright 2015, Elsevier.

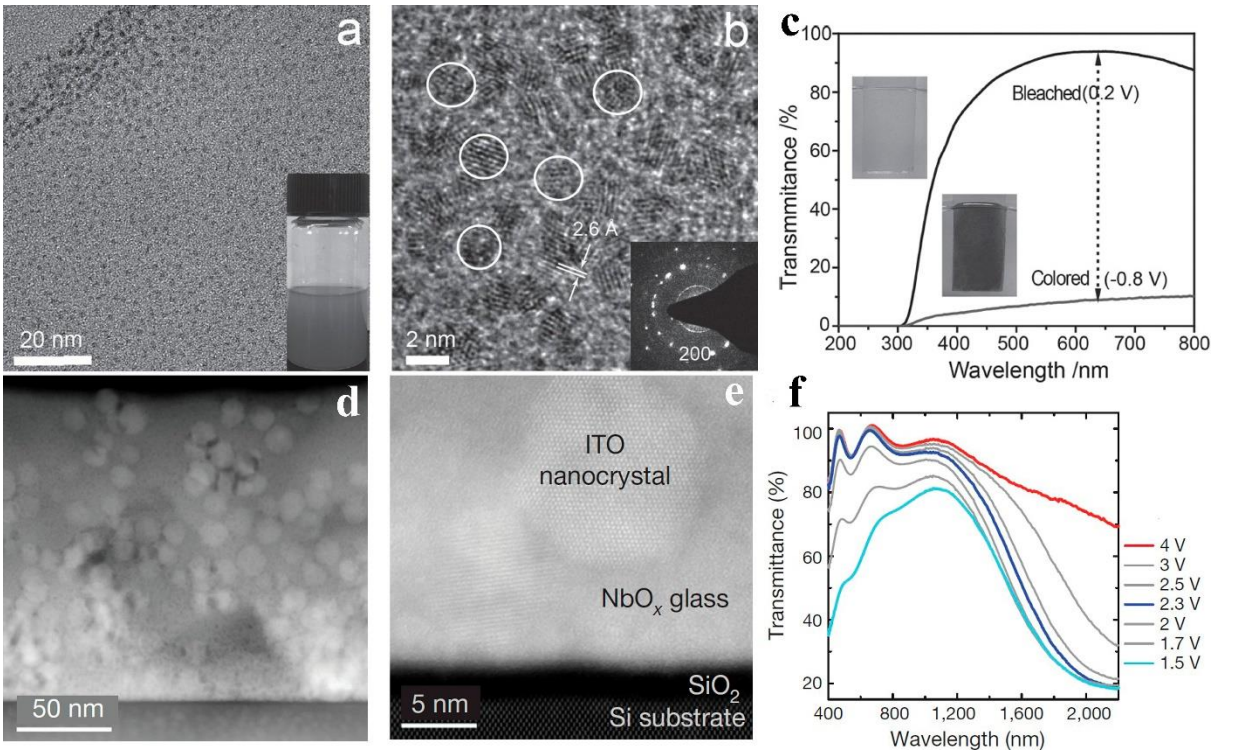

Figure 3. (a) Low- and (b) high-resolution TEM images of tungsten oxide quantum dots, Inset in (b), SAED pattern composed of individual reflected spots supporting the single crystalline nature of the tungsten oxide quantum dots. (c) Transmittance spectra of tungsten oxide QDs deposited on FTO substrate at the colored and bleached states.(a-c) Reproduced with permission.[85] Copyright 2014, Wiley-VCH. (d) Low- and (e) high-resolution cross-sectional scanning transmission electron microscopy Z-contrast images. (f) Transmittance spectra of ITO-in-NbO_x film at different states under applying different voltages, with intermediate voltages shown in grey. (d-f) Reproduced with permission.[20] Copyright 2013, Nature Publishing Group.

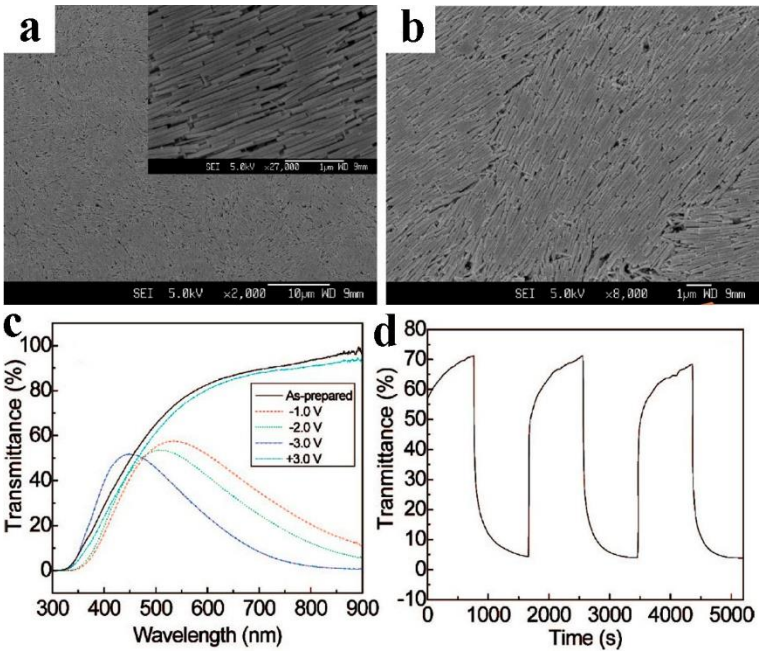

Figure 4. (a) Low magnification and (b) high magnification SEM images of the WO_3 nanorods. (c) Transmittance spectra under under applying different voltages, and (d) In situ optical responses of WO_3 nanorods film measured at a wavelength of 632.8 nm. (a-d) Reproduced with permission.[34] Copyright 2008, American Chemical Society.

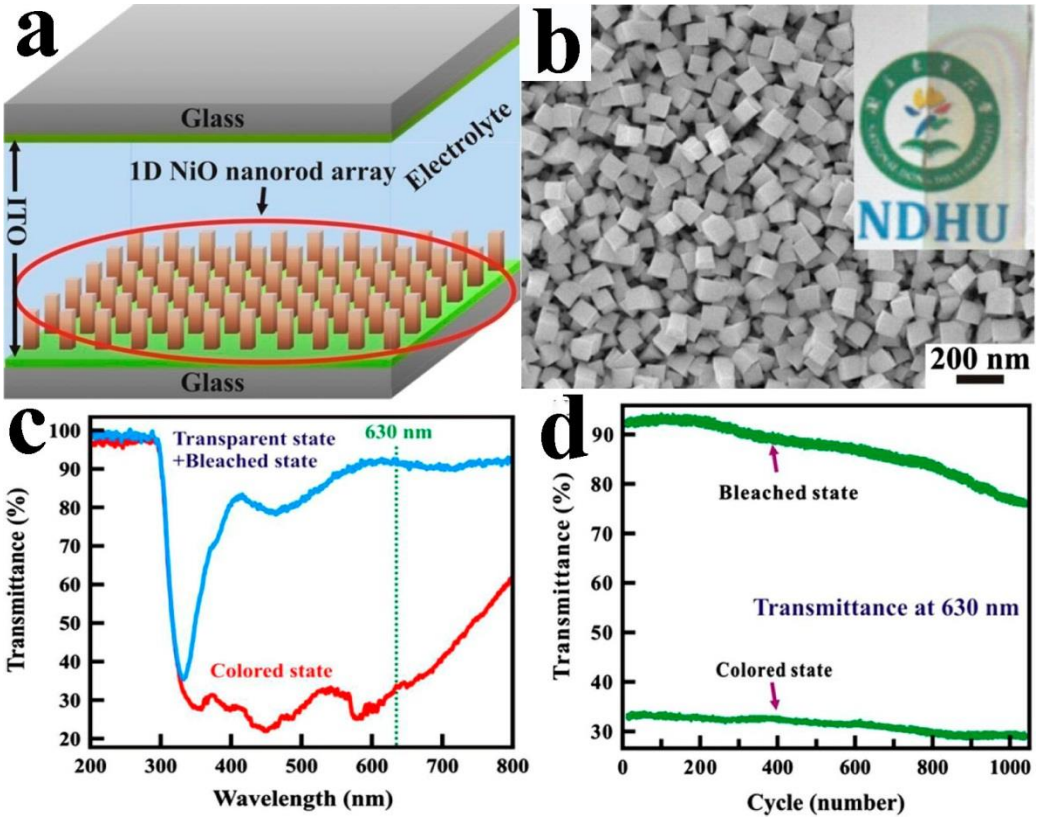

Figure 5. (a) Configuration of the NiO nanorod-based electrochromic device. (b) SEM images of top view of the large-area and highdensity array of 1D NiO nanorods synthesized on the conducting ITO thin film coated on glass, photograph inset shows that the 1D NiO nanorod array on the conducting ITO thin film is transparent. (c) Optical transmittance spectra of the NiO nanorods/ITO thin film at the colored and bleached states. (d) The stability of the 1D NiO nanorods. (a-d) Reproduced with permission.[114] Copyright 2013, Elsevier.

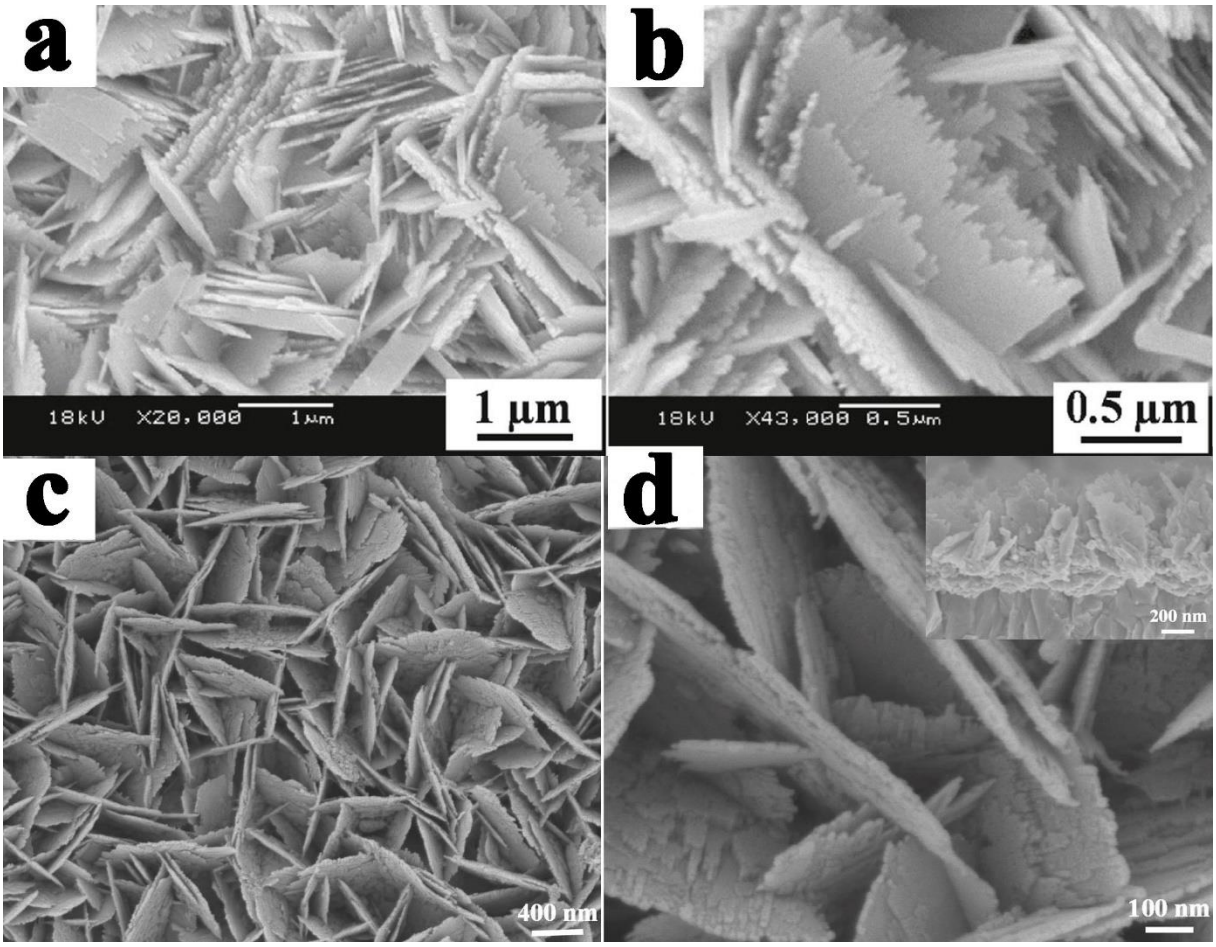

Figure 6.(a,b) SEM images of WO_3 nanosheet film grown on FTO substrate with with the assistance of WO_3 seed layer and CH_3COONH_4 capping agent. Reproduced with permission.[128] Copyright 2011, American Chemical Society. (c,d) SEM images of WO_3 nanosheet film grown on FTO substrate at pH = 1.0 condition without any capping agent assistance. Reproduced with permission.[129] Copyright 2014, Royal Society of Chemistry.

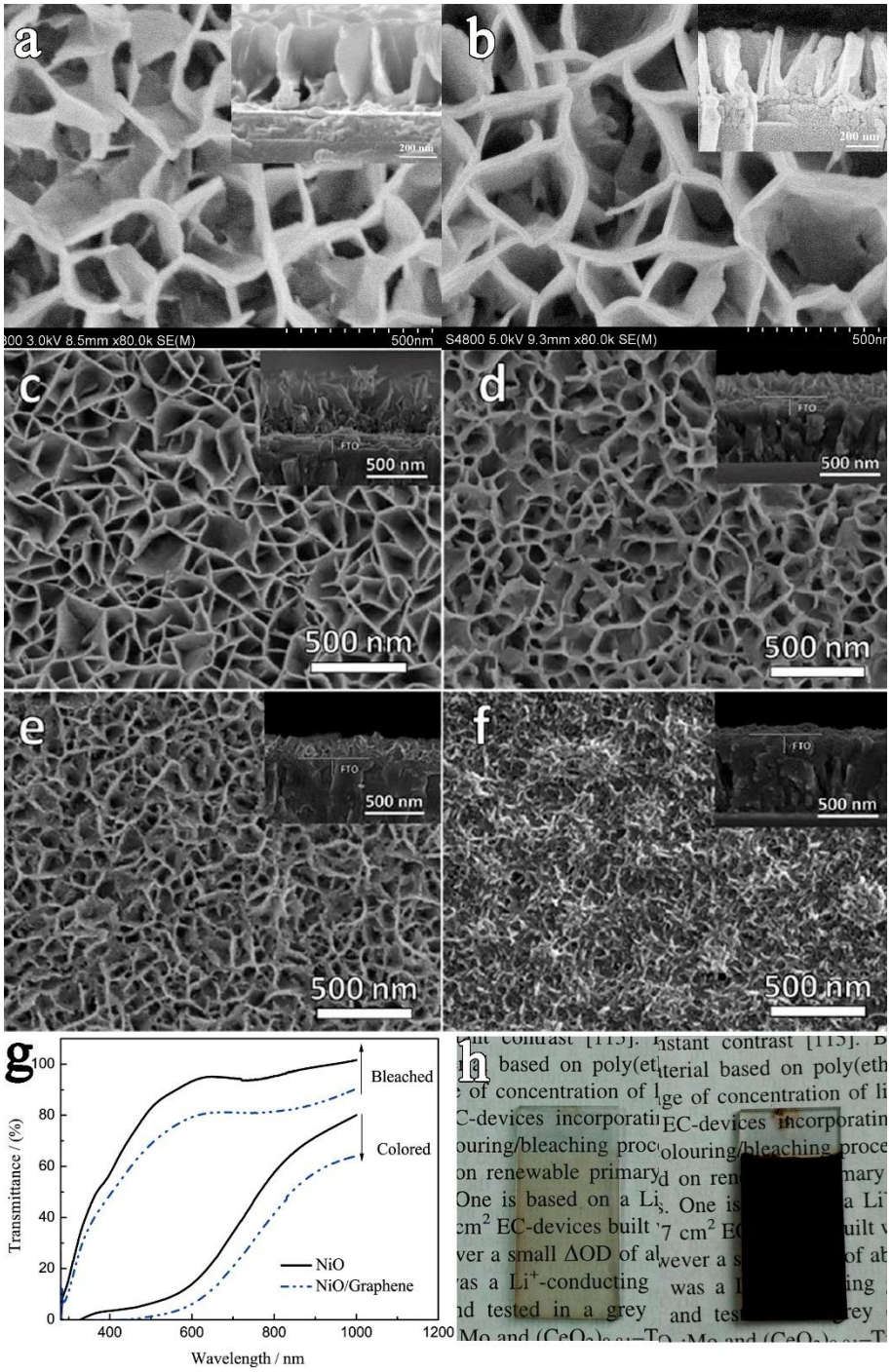

Figure 7. SEM images of (a) porous NiO nanosheet film (b) NiO/ reduced graphene hybrid nanosheet film. Reproduced with permission.[131] Copyright 2012, Royal Society of Chemistry. SEM images of Co doped NiO nanosheet with Co atomic percentage of (c) 0.3%, (d) 0.5%, (e) 1% and (f) 3%. Reproduced with permission.[132] Copyright 2014, Royal Society of Chemistry. (g) Transmittance spectra of porous NiO nanosheet film and NiO/RGO hybrid nanosheet film at colored and bleached states. (h) Photographs of the bleached and colored NiO/RGO hybrid nanosheet film. (g, h) Reproduced with permission.[131] Copyright 2012, Royal Society of Chemistry.

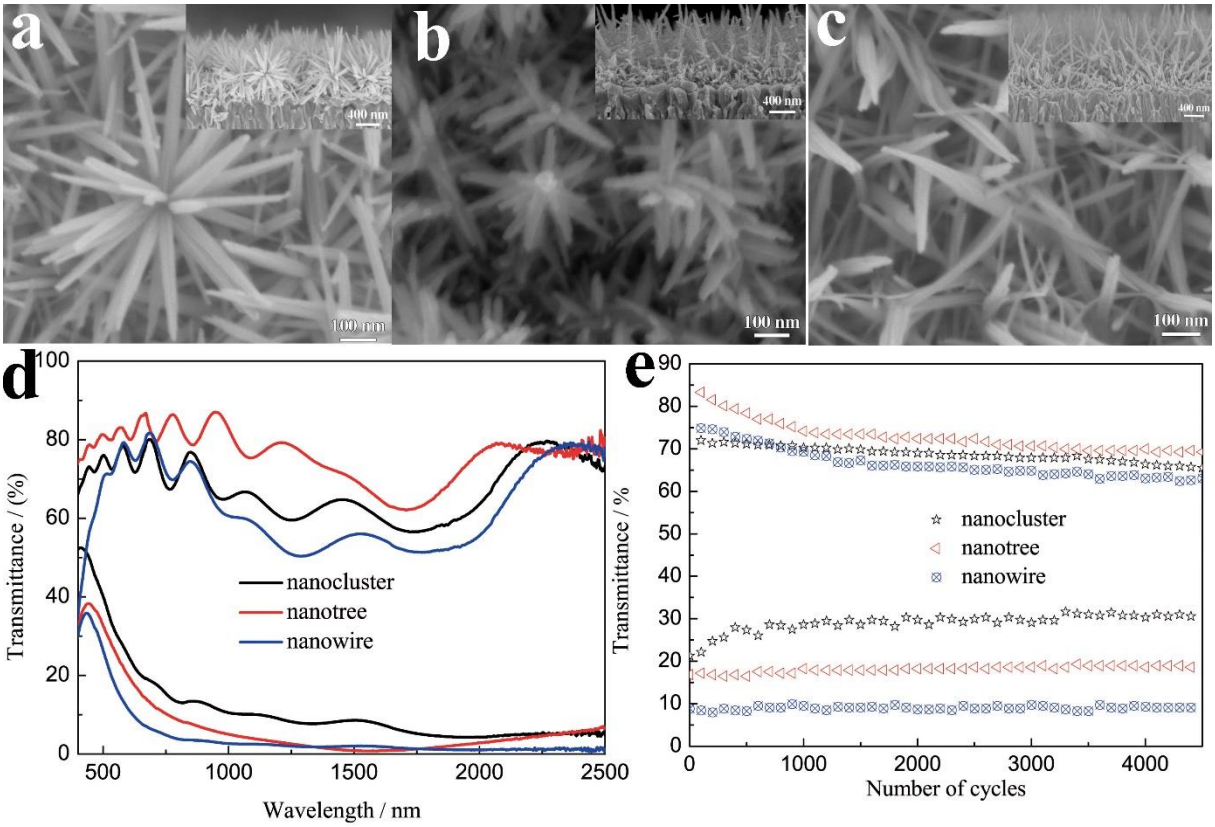

Figure 8. SEM micrographs of WO_3 films grown on FTO substrate at 200 °C for 12 h with different amounts HCl of (a) 0 μL, (b) 5 μL, and (c) 20 μL of HCl in precursor containing 60 ml absolute ethyl alcohol and 0.1 g $W(CO)_6$. (d) Transmittance spectra of WO_3 nanocluster, nanotree and nanowire array films at their colored and bleached states in the wavelength range of 400 to 2500 nm. (e) Evolution of the cycling performance of the WO_3 nanocluster, nanotree and nanowire arrays films. Reproduced with permission.[139] Copyright 2014, Elsevier.

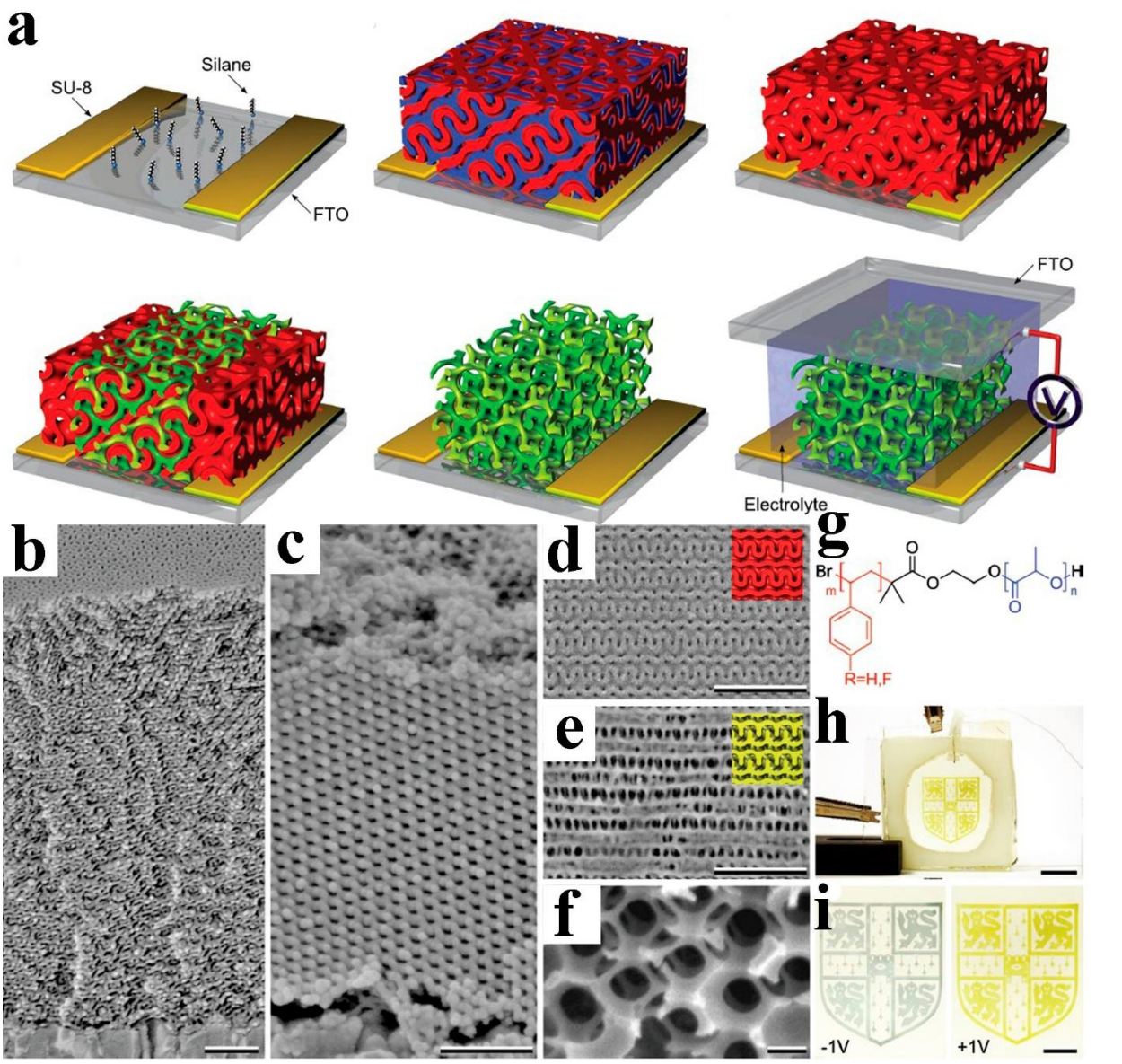

Figure 9. (a) Schematic of gyroid self-assembly, V_2O_5 replication by electrodeposition and functional electrochromic nanodevice assembled process. (b) Cross-sectional SEM graphs of mesoporous gyroid films on FTO substrates. (c) The replicated V_2O_5 after template removal. (d) The magnified free surfaces of the bicontinuous template and (e) the V_2O_5 replica. Insets displayed simulations of the double-gyroid (211) plane with a unit cell dimension of 42 nm. (f) SEM image of a macroporous V_2O_5 structure used as a reference sample. (g) Chemical structure of poly(4-fluorostyrene-*r*-styrene)-*b*-poly(D,L-lactide). All scale bars of SEM images represent 200 nm. (h) Electrochromic device with configuration of FTO/V_2O_5/$LiClO_4$+PC/FTO sequence and a Ag/AgCl reference electrode (scale bar: 1 cm). (i) Photographs of the device at bluish gray and the yellow-green colored states (scale bar: 0.5 cm). (a-i) Reproduced with permission.[61] Copyright 2012, Wiley-VCH.

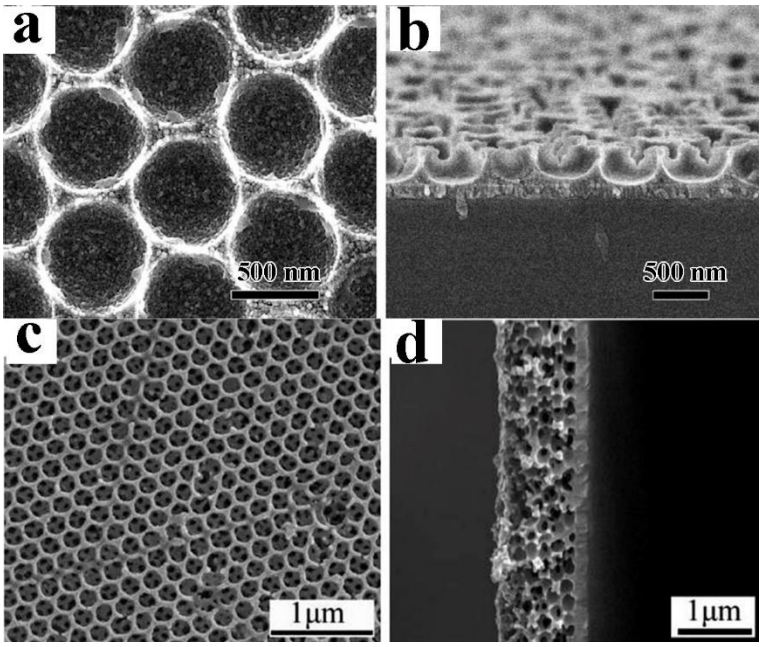

Figure 10. (a) Surface and (b) cross-sectional SEM images of macroporous WO_3 films electrodeposited using self assembled monolayer PS spheres as template. Reproduced with permission.[146] Copyright 2013, Elsevier. (c-d) Top-view and cross-section SEM images of 3DOM V_2O_5 fabricated by multilayer PS spheres as template. Reproduced with permission. [149] Copyright 2014, Royal Society of Chemistry.

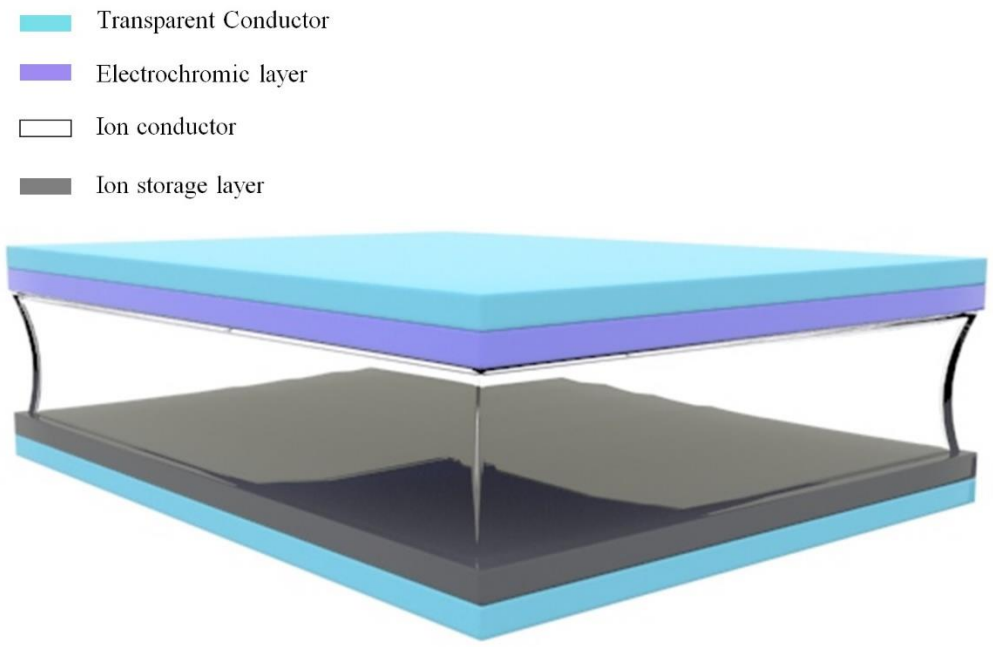

Figure 11. Configuration of a typical electrochromic smart window including two transparent conductor layers, one electrochromic layer, one ion conductor layer and one ion storage layer. Reproduced with permission.[21] Copyright 2016, American Chemical Society.

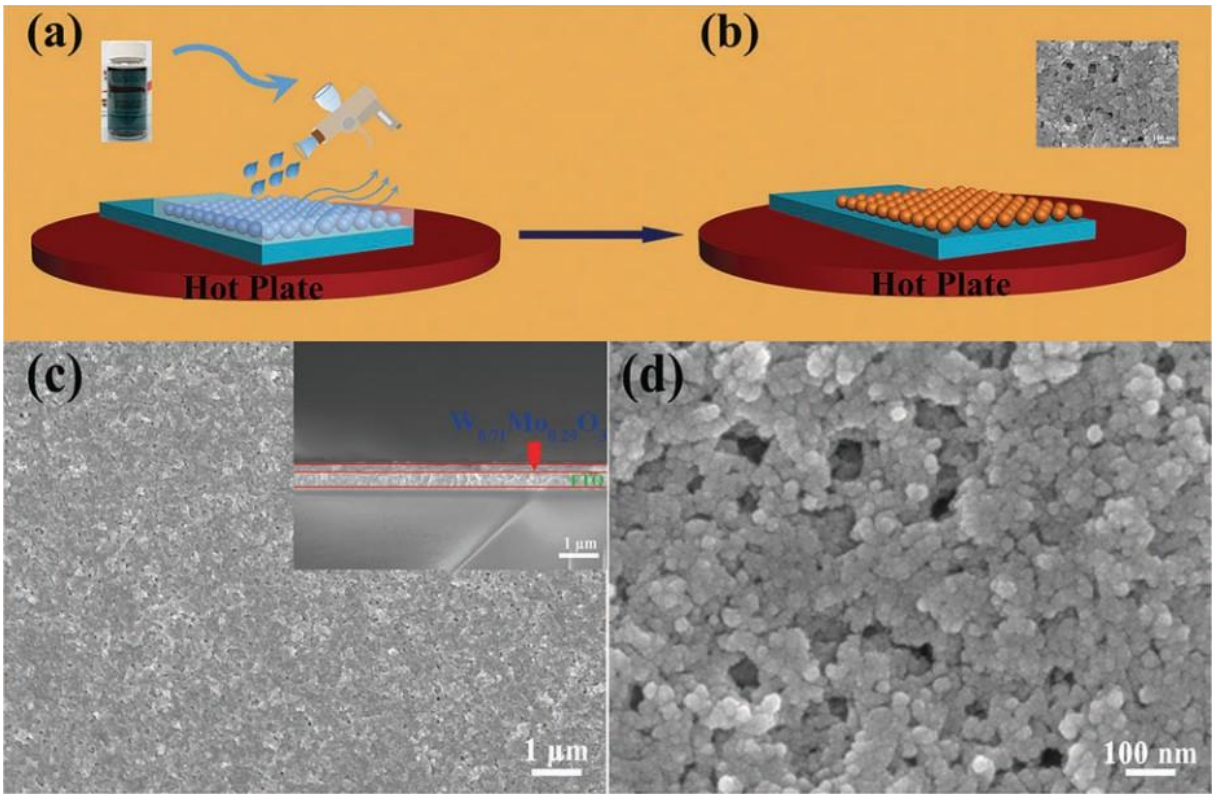

Figure 12. (a) Pale blue precursor solution sprayed on the surface of FTO glass. (b) Dried and oxidized subsequently as the droplet is sprayed onto the FTO glass. SEM images of the sprayed $W_{0.71}Mo_{0.29}O_3$ film with of (c) low magnification and (d) higher magnification. The inset in Figure 12c is the cross-sectional of $W_{0.71}Mo_{0.29}O_3$ film. (a-d) Reproduced with permission.[83] Copyright 2016, Royal Society of Chemistry.

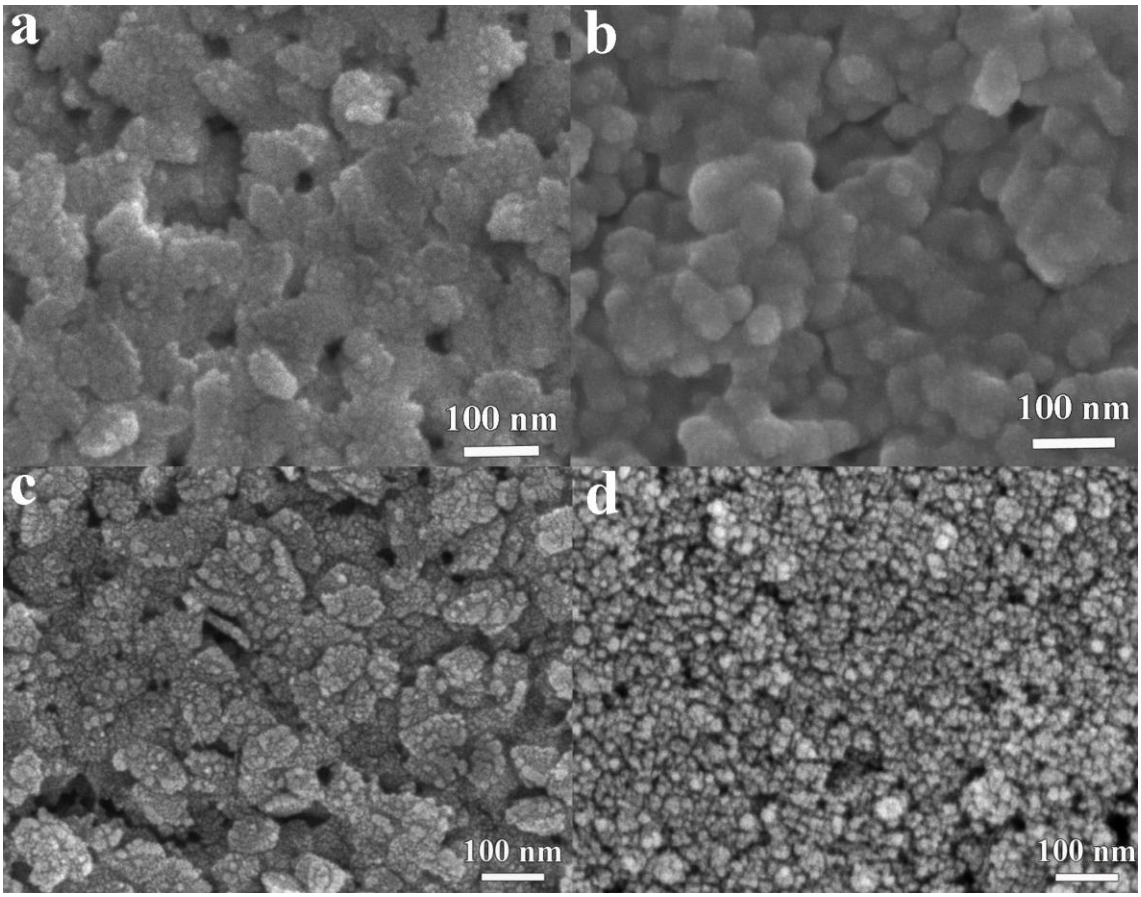

Figure 13. SEM images of inkjet printed electrochromic (a) WO_3, (b) NiO, (c) WO_3/PEDOT:PSS, (d) CeO_2/TiO_2 films. (a,b) Reproduced with permission.[156] Copyright 2016, Royal Society of Chemistry. (c,d) Reproduced with permission.[157] Copyright 2017, Wiley-VCH.

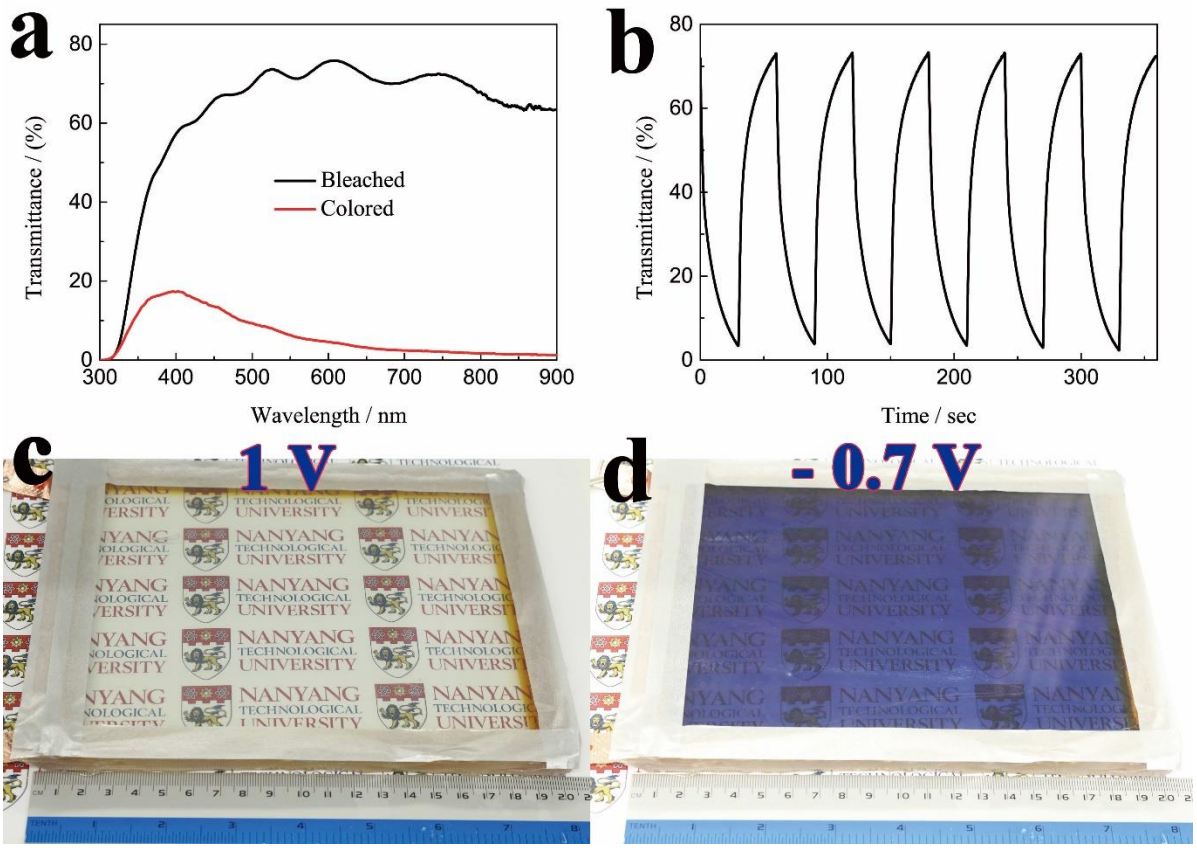

Figure 14. (a) Transmittance spectra of the large area smart window in the bleached and colored states under applying alternate potentials of −0.7 and 1 V. (b) In situ optical changes of the large smart window measured at 633 nm. (c) The digital photos of bleached and d) colored large area smart window. (a-d) Reproduced with permission.[157] Copyright 2017, Wiley-VCH.

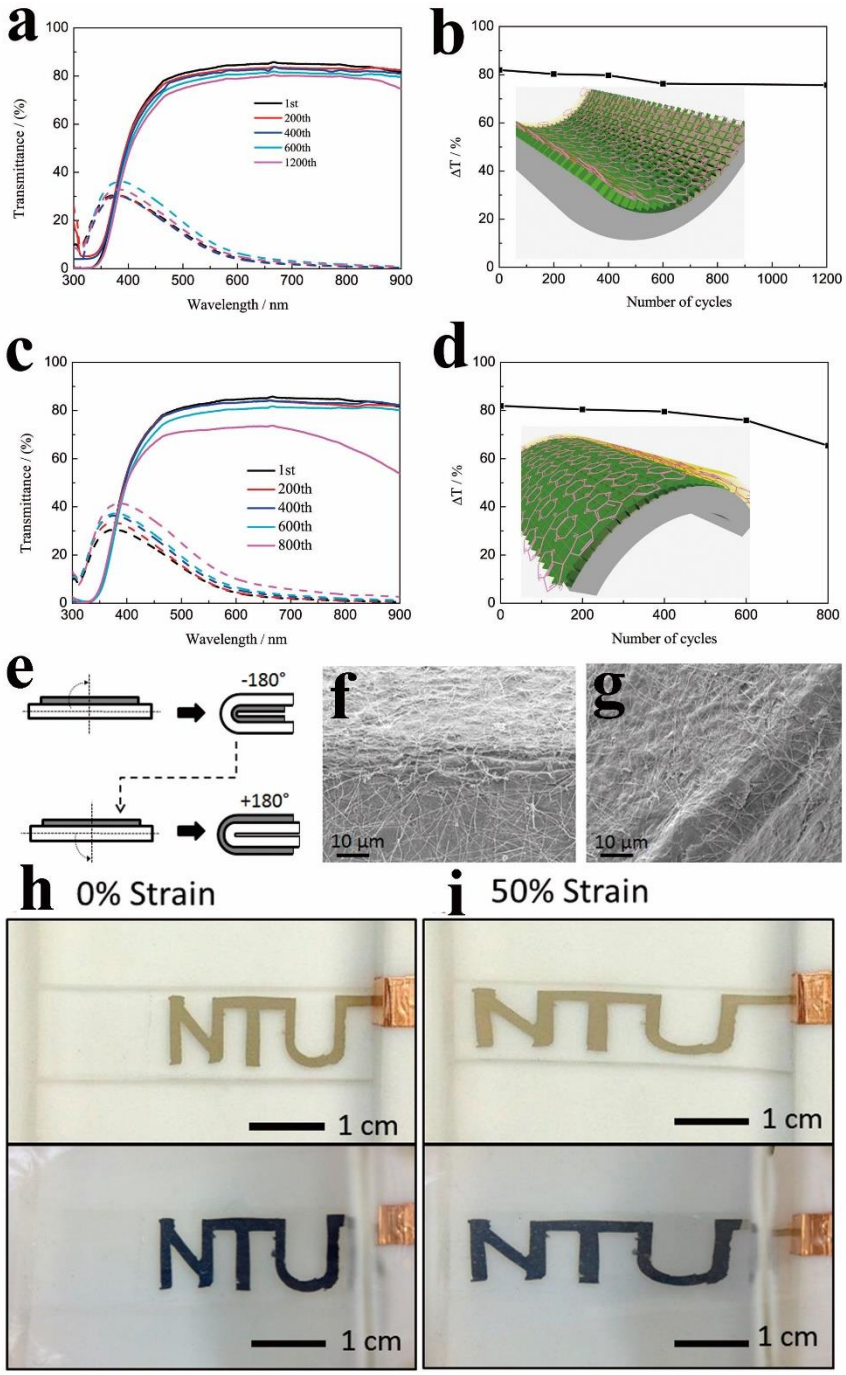

Figure 15.(a-d) Transmittance and optical modulation changes of the WO_3 nanoparticles on the flexible silver grid/PEDOT:PSS substrate under repeated compressive bending (a,b) or tensile bending (c,d) with a curvature radius of 20 mm. Reproduced with permission.[74] Copyright 2016, Wiley-VCH. (c-g) Foldability test of the nanocellulose based paper electrode. Reproduced with permission.[166] Copyright 2015, Wiley-VCH. (h, i) Digital photos of the patterned stretchable electrochromic device at bleached and colored states under 0 and 50% strain, respectively. Reproduced with permission.[169] Copyright 2013, American Chemical Society.

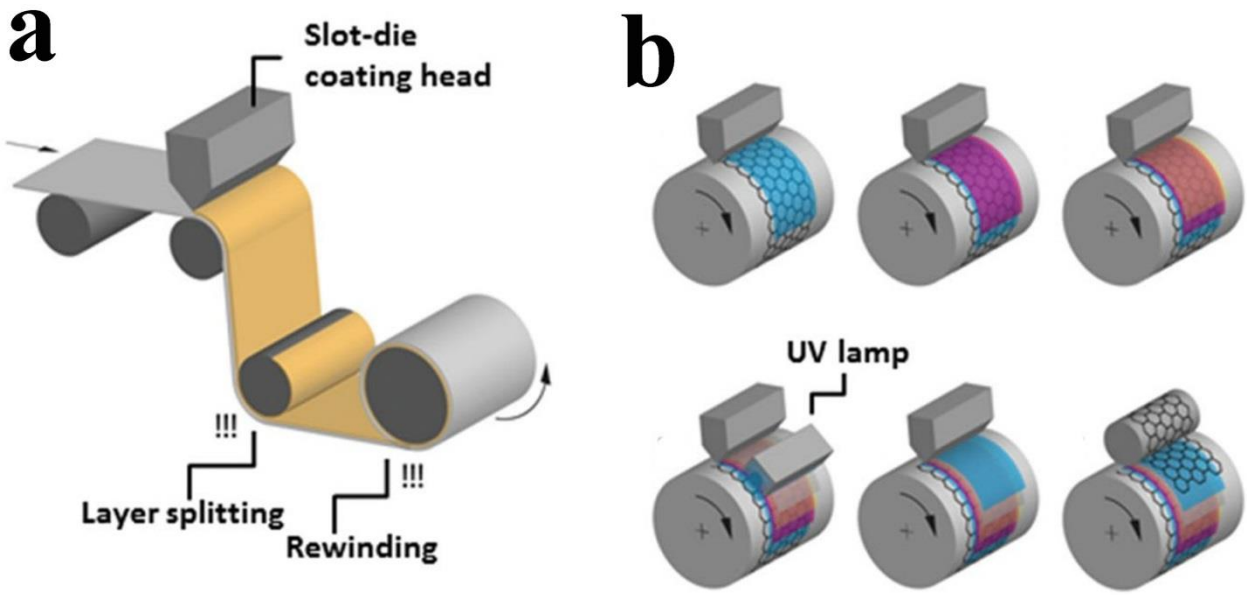

Figure 16. Integrated manufactured techniques for large scale electrochromic device preparation. Reproduced with permission.[170] Copyright 2014, Wiley-VCH.

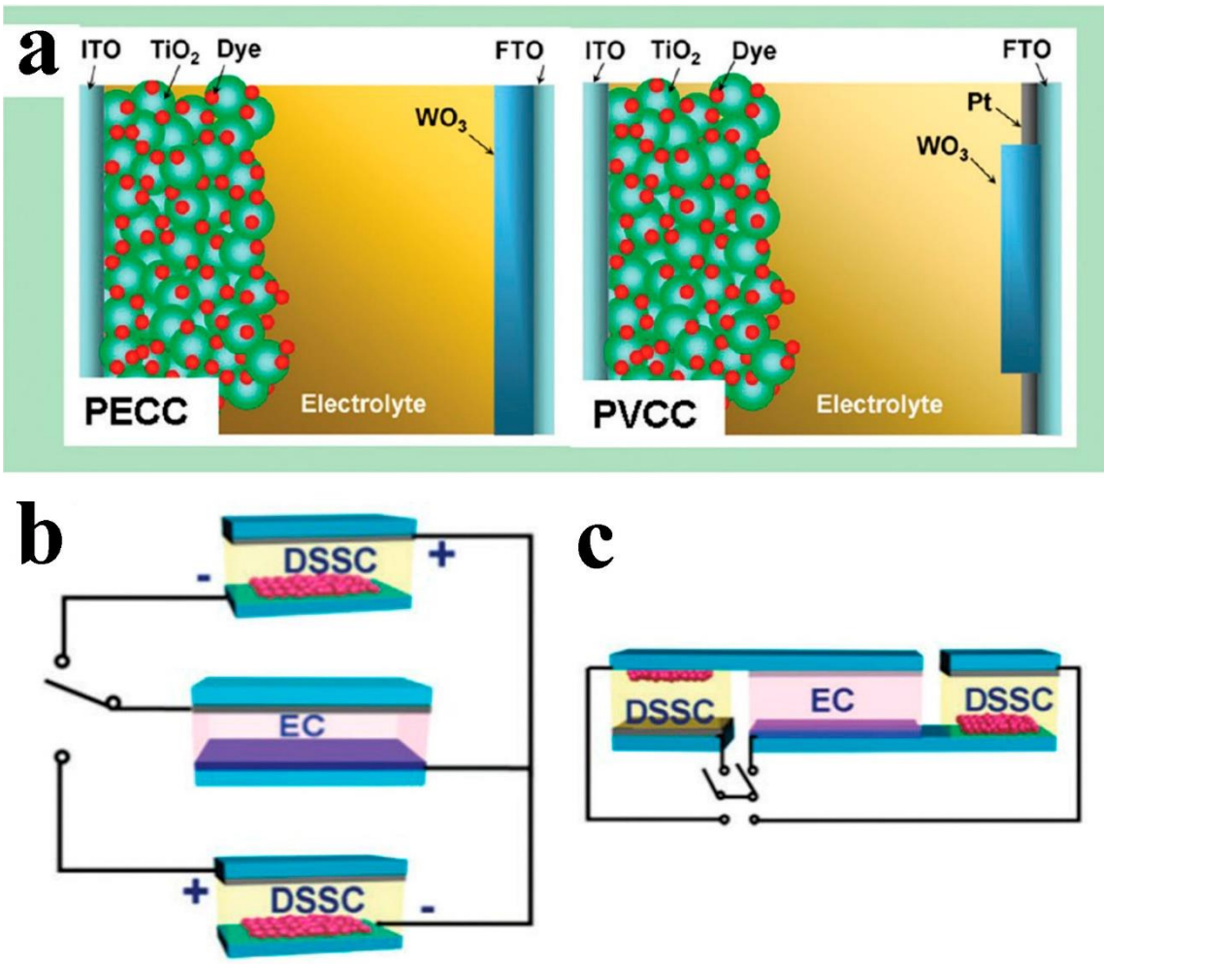

Figure 17. (a) Confirguration of PECC and PVCC devices. Reproduced with permission.[177] Copyright 2009, American Chemical Society. (b, c) Schematics of electrochromic smart window driven by dye-sensitized solar cells under illumination of sunlight: circuits of (b) the independent device and (c) the assembled device. (b, c) Reproduced with permission.[178] Copyright 2014, Royal Society of Chemistry.

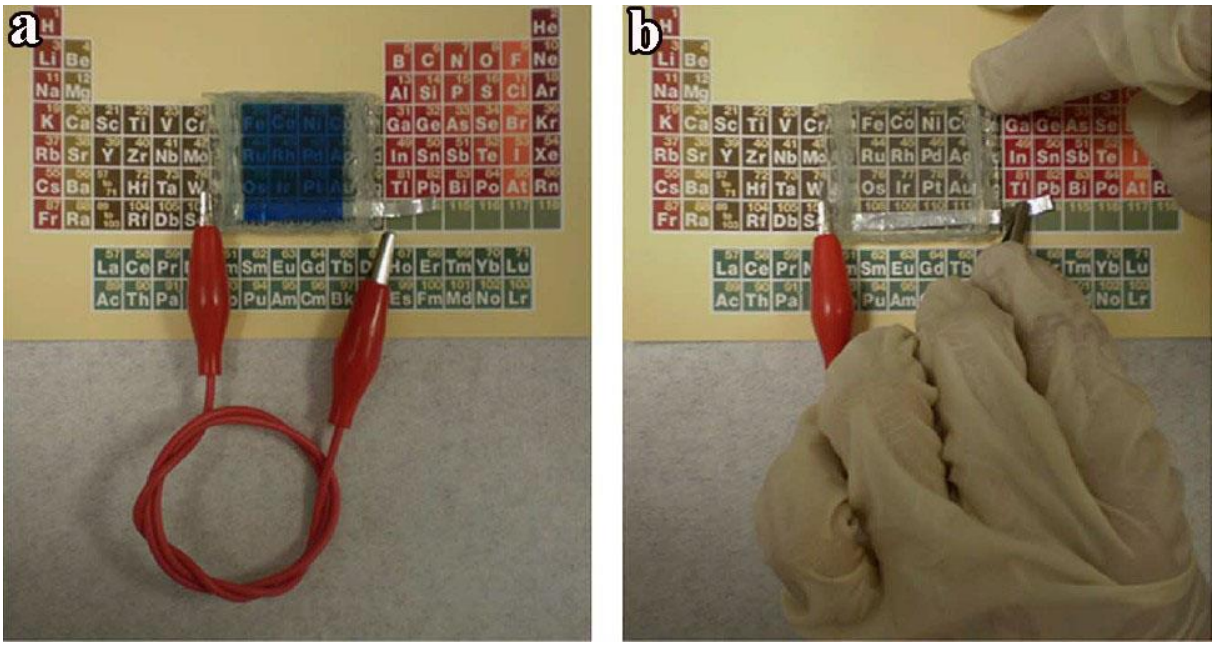

Figure 18. (a) Digital photos of the as-prepared self-powered electrochromic device with configuration of a Prussian blue layer on a piece of ITO glass, and a strip of Al sheet attached on another piece of ITO glass and 3 mol l^{-1} KCl aqueous as the electrolyte. (b) The bleached state by connecting the PB and Al electrodes. (a, b) Reproduced with permission.[185] Copyright 2014, Nature Publishing Group.

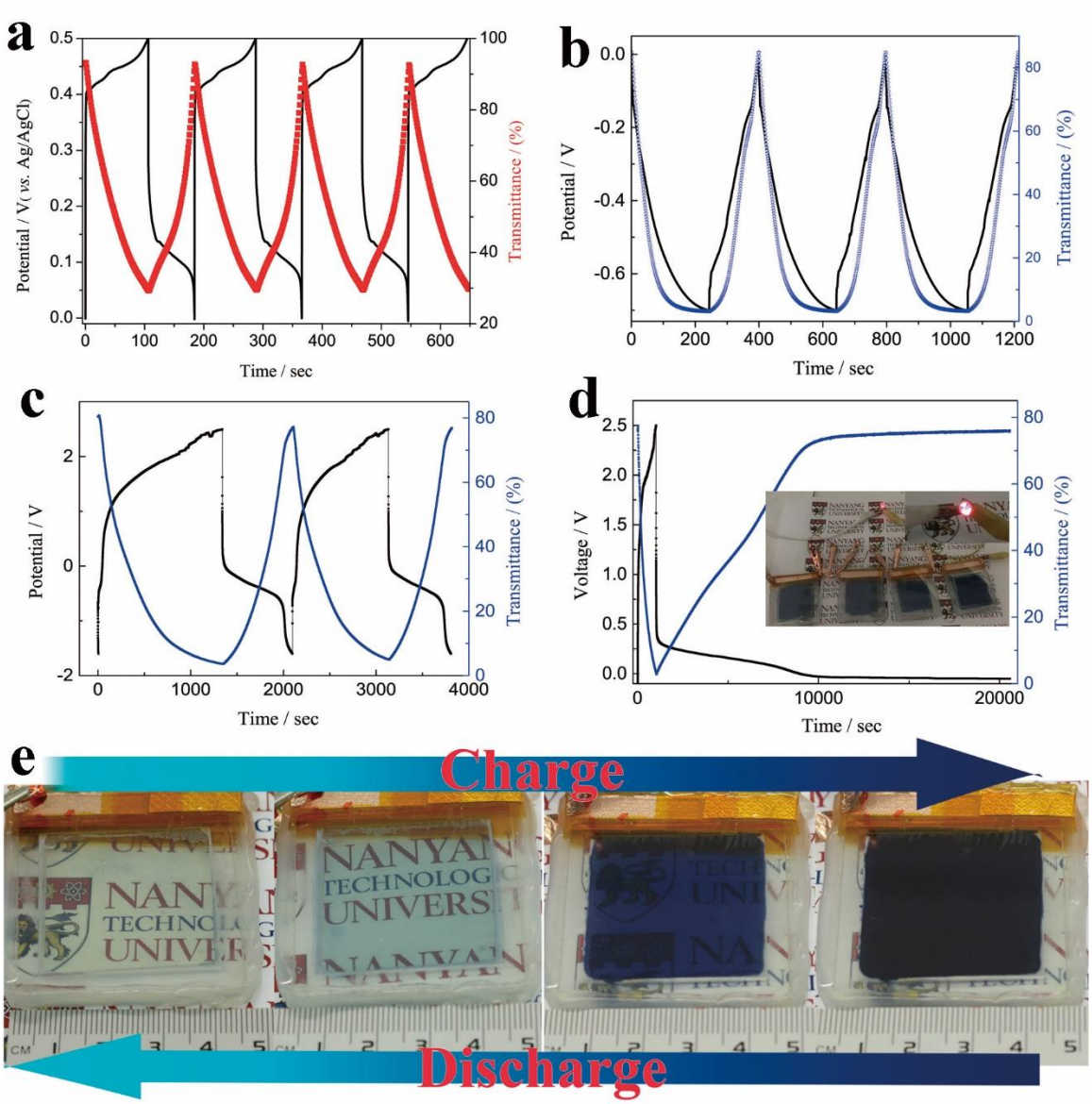

Figure 19. (a) Galvanostatic charge/discharge curves of NiO nanoparticle film on an ITO substrate measured at 2 A/g and corresponding in situ transmittance changes monitored at 550 nm. Reproduced with permission.[84] Copyright 2015, Elsevier. (b) Galvanostatic charge/discharge curves of WO_3 on silver grid/PEDOT:PSS substrate measured at at 1 A/g and corresponding in situ transmittance changes monitored at 633 nm. Reproduced with permission.[74] Copyright 2016, Wiley-VCH. (c) Galvanostatic charge/discharge profiles measured at a current density of 0.05 mA cm^{-2} and the corresponding optical changes at 633 nm for multifunctional smart window fabricated by assembling the inkjet printed WO_3/PEDOT:PSS and CeO_2/TiO_2 films as the cathode and anode, respectively. (d) Fast galvanostatic charging and slow discharging at a current density of 0.005 mA cm^{-2} and corresponding in situ transmittance changes at 633 nm for multifunctional smart window, inset displays that four small devices connected in series can light up one red LED indicators. (e) Digital photos of color transition during a charging–discharging cycle for the smart window. (c-e) Reproduced with permission.[157] Copyright 2017, Wiley-VCH.

Table of Contents Entry

Nanostructured electrochromic materials, the fabrication of large scale smart windows, rational design of multifunctional smart chromogenic devices and their performances are reviewed. Moreover, a concept of energy-efficient multifunctional smart windows is addressed in which sustainable energy can be stored in the smart windows during daytime and can be discharged to power other electronic devices at night.

Keywords

smart window, electrochromism, multifunctional device, energy storage, sustainable energy

Authors

*Guofa Cai, Alice Lee-Sie Eh, Lin Ji, and Pooi See Lee**

Title

Recent advances in electrochromic smart fenestration

ToC Figure (55 mm broad × 50 mm high)